Autoignition and preliminary heat release of gasoline surrogates and their blends with ethanol at engine-relevant conditions: experiments and comprehensive kinetic modeling

Song Cheng[1], Chiara Saggese[2], Dongil Kang[1], S. Scott Goldsborough[1*], Scott W. Wagnon[2*], Goutham Kukkadapu[2], Kuiwen Zhang[2], Marco Mehl[2], William J. Pitz[2]

[1] Energy System Division, Argonne National Laboratory, 9700 S. Cass Avenue, Argonne, IL 60439, USA
[2] Materials Science Division, Lawrence Livermore National Laboratory, 7000 East Avenue, Livermore, CA, 94551, USA

[*] Corresponding Authors:

S. Scott Goldsborough
Argonne National Laboratory
9700 S. Cass Avenue
Argonne, IL 60439
+1-630-252-9375
scott.goldsborough@anl.gov

Scott W. Wagnon
Lawrence Livermore National Laboratory
7000 East Avenue
Livermore, CA 94551
+1-925-422-2819
wagnon1@llnl.gov

ABSTRACT

This work utilizes a rapid compression machine (RCM) to experimentally quantify autoignition and preliminary heat release characteristics for blends of 0 to 30% ethanol by volume into two surrogates (FGF-LLNL and FGF-KAUST) that represent a full boiling range gasoline (FACE-F). Experimental conditions cover pressures from 15 to 100 bar, temperatures from 700 to 1000 K, and diluted/stoichiometric and undiluted/lean fuel loading conditions representative of boosted spark-ignition and advanced compression ignition engines, respectively. Direct comparison is made with previously reported results for FACE-F/E0–E30 blends. A detailed gasoline surrogate chemistry model is also proposed, and chemical kinetic modeling is undertaken using the proposed model to generate chemical insights into the compositional effects and ethanol blending effects.

Although experiments show similar qualitative trends between the surrogates, quantitative differences between the surrogates are obvious, where FGF-LLNL displays higher low-temperature reactivity and faster evolution of low-temperature heat release (LTHR) than FGF-KAUST, with such differences being significantly muted by ethanol blending. Flux analyses reveal the compositional effects on surrogate reactivity at the diluted/stoichiometric condition, where n-heptane facilitates the first-stage ignition reactivity for FGF-LLNL/E0 by initiating earlier and more rapid ȮH branching than n-butane for FGF-KAUST/E0. Sensitivity analyses highlight the importance of non-fuel-specific interactions between ethanol and surrogate sub-chemistries in controlling the reactivity of ethanol-blended surrogates. Direct experimental comparisons between the surrogates and FACE-F, as well as between the surrogate/EtOH and FACE-F/EtOH blends highlight the need of high-fidelity surrogates that can fully replicate the target gasoline in

properties including ignition reactivity and LTHR characteristics at extended conditions, as well as their response to ethanol blending. Overall, the model captures the experiments reasonably well. Nevertheless, the model displays increasing disagreement with experiments for the two surrogates at higher levels of ethanol blending, and this is found to be caused primarily by non-fuel-specific interactions between ethanol and surrogate component sub-chemistries. Furthermore, the model underpredicts the surrogate-to-surrogate differences at the diluted/stoichiometric condition, indicating a need for more physical testing on surrogates to facilitate more extensive model validation.

Keywords: Autoignition, preliminary heat release, detailed gasoline surrogate chemistry model, compositional effects, ethanol blending effects.

1. INTRODUCTION

Ethanol is the leading biofuel in transportation use. It is currently blended into commercial gasolines up to 10% in U.S., 85% in Europe, and 100% in Brazil [1]. Key benefits of ethanol-blended gasolines include the enhanced anti-knock performance [2] and reduced NO_x [3], carbon monoxide (CO) and particulate matter (PM) [4] which are regulated emissions. Such benefits have led to favorable energy policies, e.g. RFS2 (Renewable Fuel Standard) [5], that seek to further increase ethanol use in transportation fuels. Additionally, the U.S Department of Energy Co-Optima Initiative has recently identified ethanol as one of the top-10 blendstocks that present the smallest barriers to near-term adoption for modern downsized, boosted spark-ignition (SI) engines [6]. Integrating ethanol as part of a near-term transition to low carbon intensity fuels requires greater fundamental understanding of the autoignition characteristics of ethanol-blended gasolines.

Generating consistent, fundamental understandings of gasoline oxidation is challenging due to the compositional complexity, and wide variability of petroleum-derived, full-boiling range gasolines, and this has led to different findings of ethanol blending behaviors (e.g., synergistic response with U.S. gasolines [7] but a somewhat linear blending effects with an Australian gasoline [8] on volume basis). Greater, and consistent insight can be gained however, by using gasoline surrogates with significantly fewer, invariant components that are able to reproduce a range of chemical and physical properties of real gasolines. The use of gasoline surrogates with limited diversity also considerably reduces the number of species formed during the course of oxidation, enabling computational fluid dynamic simulation of practical combustors and development of chemical kinetic models that are generally suitable for engineering applications.

Historically, binary blends of n-heptane and iso-octane, termed primary reference fuels (PRF), have been used as the simplest gasoline surrogates for octane ratings in the standardized American Society for Testing and Materials (ASTM) tests for research octane number (RON) [9] and motor octane number (MON) [10]. Ternary blends of n-heptane, iso-octane and toluene (i.e., TRF) have also been proposed as gasoline surrogates to achieve a better reproduction of octane sensitivity (RON minus MON, denoted as S) [11, 12]. However, modern engine development, and the growing need to better understand and model the complex underlying chemistry of gasoline combustion require surrogates to capture additional properties beyond octane numbers and S, including C/H ratio [13-15], PIONA (paraffins, isoparaffins, olefins, naphthenes, and aromatics) [13-15], carbon types [15], distillation curve/volatility [15, 16], etc. These additional properties are not able to be adequately replicated by simple surrogates such as PRFs and TRFs, and require use of multi-component surrogate formulations.

It is important to recognize that understanding fuel behavior across a variety of combustion scenarios is important to address technical barriers to engine design, in a collaborative, efficient manner. This is challenging with commercial gasolines due to their compositional complexity and variability. Thus, the use of research-grade gasolines with consistent composition can be preferable, even if they do not exactly match some of the standardized fuel properties. While numerous efforts have been performed to formulate multi-component surrogates for various gasolines, this study focuses on FACE (fuels for advanced combustion engines) gasoline F, which was developed by the Coordinating Research Council [17] to replicate specific property targets. and facilitate consistency across different research investigations. Recently, Lawrence Livermore National Laboratory (LLNL) and Sarathy et al. [18] created 5-component and 7-component

surrogates for FACE-F, denoted as FGF-LLNL and FGF-KAUST, respectively. These surrogates match not only RON and MON of the original gasoline but also several additional gasoline properties via a palette of components determined based on the results of detail hydrocarbon analysis (DHA) [17].

Several studies have evaluated the performance of FGF-LLNL and FGF-KAUST in replicating FACE-F. Knock limited advance spark measurements were conducted in a cooperative fuel research engine for FGF-KAUST and FACE-F [18], where the surrogate accurately captured the change in knocking intensity as a function of spark timing under both RON-like and MON-like conditions. The autoignition characteristics of both FGF-LLNL and FGF-KAUST were later evaluated and compared with FACE-F as well as two simpler surrogates (PRF and TRF blends) by Kang et al. [19] in a Rapid Compression Machine (RCM) under extended conditions that are more representative of boosted spark-ignition (SI) and advanced compression ignition (ACI) engines. They found that the two multi-component surrogates displayed similar autoignition behavior across the conditions studied, and captured the pressure and temperature dependences in the ignition reactivity of FACE-F better than the PRF and TRF surrogates, particularly at lean conditions where the PRF and TRF failed to display pronounced negative temperature coefficient (NTC) behavior. Jet-stirred reactor (JSR) oxidation of FACE-F was studied by Chen et al. [20] at temperatures covering 500 – 1200 K and equivalence ratios of 0.5, 1.0 and 2.0, where simulations were conducted with FGF-KAUST and FGF-LLNL. Excellent agreement between the simulation and experiments in fuel consumption was observed at stoichiometric condition, despite the over-predicted low- and high-temperature reactivity at lean and rich conditions, respectively. Chen et al. [21] further reported JSR results of FGF-KAUST at similar conditions and compared to the

results for FACE-F reported in [20]. They found that FGF-KAUST demonstrated similar oxidation behaviors to FACE-F. Recently, insights into the autoignition characteristics of FACE-F/EtOH blends were reported by Cheng et al. [22] in an RCM at engine-relevant conditions. Variable-volume simulations were also conducted with FGF-LLNL, and they found that the simulation results captured well the measured ignition trends of 'neat' FACE-F where 'neat' is defined here as the absence of ethanol. Studies on the octane response of FACE-F/EtOH blends [23] and the combustion characteristics of terpineol-blended FACE-F [24] have also been reported, but there were no comparison to FACE-F surrogates.

Ethanol blending effects are complex since ethanol can perturb the base fuel chemistry in various ways. For instance, it has been reported that ethanol favors ȮH termination pathways forming acetaldehyde and hydroperoxyl radicals over conventional low-temperature chain branching pathways that are typically seen for petroleum-derived gasoline constituents [25-27]. Also, ethanol has been observed to show synergistic blending effects on octane number with *n*- and *iso*-paraffins [23], while antagonistic blending effects with aromatics [28]. Due to such differences, ethanol blending effects are often non-linear and greatly depend on the compositional distribution of the base gasoline. Understanding of the underlying chemical interactions between ethanol and the base gasoline components, beyond just perturbations to the radical pool, is necessary when blending behaviors are to be predicted via surrogates, for both conventional engine operation, as well as ACI combustion schemes. However, current formulation strategies/methodologies for multi-component surrogates, e.g., FGF-LLNL and FGF-KAUST, target only base gasolines without accounting for potential kinetic interactions with blending agents such as ethanol [29]. As a result, although FGF-LLNL and FGF-KAUST demonstrate

good correspondence with FACE-F across a wide range of operating conditions, it has not been experimentally demonstrated to what extent they are able to capture the ethanol blending effects on FACE-F.

Equally important is the accuracy of the kinetic models since surrogates are now generally formulated using a computational perspective with kinetic models as a foundational tool [13-16, 18, 29]. However, the kinetic models used to formulate the surrogate are often not validated experimentally for the surrogates, or for their blends with ethanol. Instead, the models are typically validated for individual compounds, e.g., n-heptane or iso-octane, or binary blends, and this may not be sufficient for predicting multi-component surrogate behaviors since nonlinear interactions between the surrogate components and those with ethanol are overlooked. As a result, the physical surrogates formulated based on predictions of such models can behave differently from real gasolines. Recently, Cheng et al. [22] found that the disagreement between experiments for FACE-F/EtOH blends and modeling results using FGF-LLNL/EtOH blends became greater with higher levels of ethanol addition. Due to the lack of model validation directly against FGF-LLNL/EtOH experiments, it is unclear if such disagreements are introduced by the inaccurate FGF-LLNL/EtOH chemistry in the model, or the inability of FGF-LLNL to properly replicate ethanol blending effects on FACE-F. Ascertaining this requires direct comparison of experimental results between FACE-F/EtOH and the surrogate/EtOH blends, though these are not currently available in the literature.

The objective of this work is twofold. Specifically, we seek to: 1) experimentally reveal compositional effects of ethanol blending on the autoignition and heat release characteristics of FGF-LLNL and FGF-KAUST at engine-relevant conditions, and compare these with ethanol-

blending responses observed with FACE-F, as reported in [22]; and 2) better understand the underlying chemistry responsible for ethanol-blending effects, including influences of fuel composition, and thus the fidelity needed in 'neat' surrogates in order to properly replicate target gasolines. Insight into these issues is expected to shed light on challenges that lie with current multi-component surrogate formulation strategies/methodologies, and chemical kinetic modeling of full boiling range gasolines.

Towards this, new measurements are conducted for FGF-LLNL/EtOH and FGF-KAUST/EtOH blends using an RCM, where ethanol concentration is varied from 10% to 30% by liquid-volume. Experimental results for FACE-F/EtOH blends are taken from [22] for direct comparison with the surrogate/EtOH blends. Two fuel loading conditions are used, one that represents stoichiometric diluted/boosted SI engine operation and another representing undiluted/lean ACI operation, with each covering a range of engine relevant conditions with pressures from 15 to 100 bar and temperatures from 700 to 1000 K. Changes in overall reactivity and heat release behavior are both quantified and compared across the different blends. A recently-updated, detailed gasoline surrogate model from Lawrence Livermore National Laboratory (LLNL) is proposed and used to model the RCM experiments, providing insight into the differences in perturbative behaviors for the two gasoline surrogate blends.

The remaining manuscript is organized as follows. Section 2 provides a description of the experimental facility used for data acquisition as well as the methods used for post-processing and kinetic modeling in this study. Section 3 discusses the experimental and modeling results at the two fuel loading conditions. This is followed by a summary of the paper in Section 4.

2. EXPERIMENTAL AND COMPUTATIONAL METHOD

2.1. Surrogate formulation and preparation

Two multi-component FACE-F surrogates, namely FGF-LLNL and FGF-KAUST, are used for this work. Detailed philosophies to develop these surrogate blends, including selection of appropriate target properties and corresponding surrogate mixtures can be found in [30] for FGF-LLNL and in [15, 31] for FGF-KAUST, hence only key features are described here. Mehl et al. [30] numerically formulated the five-component FGF-LLNL with each constituent selected from a palette containing five structural families where carbon type, molar H/C ratio, anti-knock index (AKI) and octane sensitivity (S) were target properties selected. Two correlations were utilized to estimate AKI and S: first, between homogeneous gas-phase ignition delay times at 825 K and 25 atm and AKI; and second, between the minimum slope of the NTC region and S. On the other hand, FGF-KAUST is a seven-component surrogate formulated by matching the RON, MON, PIONA, C/H ratio, carbon types, average molecular weight, density, and distillation characteristics [15, 31] of FACE-F. An objective function representing the difference between the target properties of the FACE-F and the proposed mixtures was minimized to determine the optimal surrogate composition, where the RON and MON of the mixtures were calculated based on linear blending rules of the palette compounds. The compositional makeup and target properties of FGF-LLNL and FGF-KAUST are compared to FACE-F in Tables 1 and 2, respectively, while detailed chemical and physical properties of FACE-F can be found in [17].

It can be seen in Table 2 that FGF-KAUST provides better matching of physical properties compared to FGF-LLNL, due to better mimicking of aromatics, olefins, and naphthenes, as shown in Table 1. The concentration of these compounds greatly affects C/H ratio and S of the surrogate blend.

Table 1. Composition of FACE-F [17], FGF-LLNL [30] and FGF-KAUST [31], listed as molar percent.

Structural Family	FACE-F	Palette Compound	FGF-LLNL	FGF-KAUST
n-**P**araffins	4.8	*n*-Butane	0	6.9
		n-Heptane	7	0
I*so*-paraffins	61.0	2-Methyl butane	0	9.8
		2-Methyl hexane	0	7
		Iso-octane	53	43.7
Olefins	10	1-Hexene	14	8.4
Naphthenes	15.8	Cyclopentane	14	15.8
Aromatics	8.4	Toluene	12	0
		1,2,4-Trimethylbenzene	0	8.4

Table 1. Properties for FACE-F and its two surrogates, FGF-LLNL and FGF-KAUST.

Properties	FACE-F	FGF-LLNL	FGF-KAUST
RON	94.4[a]	93.8[b]	93.6[c]
MON	88.8[a]	89.5[b]	88.9[c]
AKI*	91.6	91.6	91.5
S*	5.6	4.3	4.7
Density at 288 K (kg/m^3)	707	712	707
C/H ratio	0.469	0.485	0.472
Avg. mol. Wt. (g/mol)	94.8	100.2	96.2

[a] RON and MON measured in [17];
[b] RON and MON estimated using correlations from [30];
[c] RON and MON estimated using correlations from [15];
* Anti-Knock Index (AKI) = (RON+MON)/2; Sensitivity (S) = RON-MON

Surrogate samples are prepared by the following procedures. Mole fractions of the surrogate components (listed in Table 1) are converted to volumetric fractions for a total volume of 30 ml. Perfect mixing behavior is assumed with no excess volume effects. Each component is then prepared using a syringe, according to the volumetric fractions, and is injected into a 50 ml, pre-weighed sample vial. The vial is weighed after each injection, using a Denver instrument A-160 balance with a resolution of 0.1 mg, to determine the masses of the individual components, which are used to compute the mole composition of the surrogate blend. Calculated mole fractions (listed in Table S1 in the Supplementary Material) agree well with the targeted mole

fractions listed in Table 1, within an average variability of ±0.87%. It should be noted that FGF-KAUST contains n-butane and this is supplied to the mixing tank separately in vapor phase from a stationed lecture bottle, which is discussed in Section 2.2.2.

2.2. Rapid compression machine

2.2.1. Description

A heated, twin-piston RCM (tpRCM) at Argonne National Laboratory (ANL) is utilized for this study. A detailed description of the configuration as well as uncertainties associated with experimental measurements can be found in [32], and is briefly provided here. A single compression event is driven by the pneumatic system, and a hydraulic pin-groove arrangement is used to arrest the fast-moving pistons, allowing them to be hydraulically locked at the end of compression. The time for compression (t_{comp}) and last 50% of pressure rise (t_{50}), are approximately 15–18 ms and 1.9–2.0 ms, respectively, with higher compressed pressure (P_C) leading to longer slightly t_{comp} and t_{50}.

The reaction chamber and the two compression cylinders have an inner diameter of 50.8 mm, with a clearance height of nominally 25.5 mm at the end of compression. The stroke for each reaction chamber piston is 155.8 mm such that the geometric compression ratio (CR) is constant at 12.1:1, while compression heat loss results in an effective compression ratio ranging from 11.2:1 to 11.8:1, depending on the compressed state conditions, primarily Pc, and inert diluent conditions that affects the specific heat ratio of test mixture. The pistons utilize crevices machined around their circumference [32] to suppress possible vortex roll-up during the

compression, thus improving post-compression charge homogeneity. The dynamic pressure in the reaction chamber is measured using a flush-mounted Kistler 6045A-U20 pressure transducer calibrated to 250 bar, and coupled to a Kistler Type 5064 charge amplifier. The transducer has a reinforced diaphragm for applications at excessive pressure rise rates. The thermal shock error of the transducer is estimated at $\Delta P_{max} < \pm 1\%$, and is used uncoated.

To accurately capture two-stage exothermic characteristics, the pressure signal can be split and recorded using two different National Instruments (NI) data acquisition cards. Since the first-stage heat release features much lower heat release rates, a 24-bit card is used for this study (NI 9239), sampled at 50 kHz. Higher rates of heat release, e.g., through the high temperature heat release (HTHR) process, are more robustly captured with a 16-bit card (NI 9223) sampled at 1 MHz. Goldsborough et al. [33] identify data acquisition and post-processing issues associated with heat release rate calculations. The pressure signal is filtered using the Savitzky-Golay algorithm with a second-order polynomial fit over a window of 0.2 ms (i.e., 11-point window for the 50 kHz data).

2.2.2. Mixture preparation

Mixtures of fuel, diluents (Ar and N_2), and O_2 are prepared in a 5.6 L, stainless steel tank, which is electrically heated to ~70 °C, and initially purged with inert gas and evacuated to < 0.1 mbar using an Edwards nXDS6i vacuum pump. A pre-determined mass of the liquid surrogate blend is first introduced into the tank through a septum, and then high-purity gases are supplied into the tank in the sequence of Ar (99.9997%, Airgas), N_2 (99.9998%, Airgas) and O_2 (99.9997%,

Airgas). For mixtures containing FGF-KAUST, n-butane is supplied directly to the mixing tank, after the liquid fuel sample is injected, but before diluents are introduced, to the required partial pressure, which is calculated using the mass of the liquid surrogate blend injected and the targeted mole fraction of n-butane in FGF-KAUST, i.e., 6.9%. Six batches of each mixture were made for FGF-KAUST tests, where the n-butane mole fraction slightly varies within an average variability of ±1.28%. The mole percent of n-butane for each batch can be found in Table S2 in the Supplementary Material.

The manual filling valves placed upstream of the mixing tank inlet allow gases to be metered to within ±3 mbar of the desired value. Each feed requires an interval waiting time of 3–5 minutes to equilibrate the pressure of the tank, which is monitored using an MKS Baratron 628F (0–6666 mbar) heated manometer with a manufacturer specified uncertainty of ±0.25%. After completion of each test batch, the mixture in the tank is isolated for at least 45 minutes to diffusively mix. Variations in the wait time has been explored, up to 3 h, with no noticeable change observed in measured ignition delay times. The evaporation efficiency of the liquid fuel is calculated based on ideal gas relations and is >95%, while the molar composition of the mixture is estimated from the partial pressure of gaseous components and the mass of fuel injected.

2.2.3. Experimental procedure

The surfaces of the reaction chamber and cylinders are heated to the desired temperature using electrical heating tapes with high-density insulation fitted between the flanges of the cylinders and the hydraulic chambers. The temperature on the outside surfaces of the reaction

chamber and cylinders is periodically monitored using K-type thermocouples placed at 16 different positions along the cylinder and chamber surfaces. Thermal uniformity of ±0.2% is achieved in the axial and azimuthal directions across the interior and exterior surface with at least 45 min of wait time. The reaction chamber is then evacuated and purged several times using dry, bottled air (99.998% purify Airgas) before each filling event. The reaction chamber pressure is monitored using an MKS Baratron 628F (0–6666 mbar) heated manometer with a manufacturer specified uncertainty of ±0.25%. The test mixture is supplied into the reaction chamber to the targeted initial pressure using a MKS 248A-11094 electronic flow control valve through Polytetrafluoroethylene (PTFE)-lined and stainless-steel tubing heated to approximately 70 °C. A proportional-integral-derivative (PID) controller is implemented in the LabVIEW control system in order to automate the filling procedure and control the reaction chamber pressure to within 0.15% of the desired value. After each filling event, the test mixture is allowed to equilibrate for at least 5 minutes in the chamber before commencing the test. A minimum of two shots were conducted at each compressed state to ensure repeatability. For these tests, repeatability was evaluated based on a number of factors, including compression time, time needed for the last 50% of pressure rise, the compressed thermodynamic condition (T and P), the first-stage and main ignition delay times, and pressure rise rates and peak pressure at main ignition.

2.2.4. Data Analysis Processing

The compressed temperature (Tc), ignition delay times and heat release rates are determined by post-processing recorded pressure traces. In order to ascertain the end of

compression (t_0) and the extent of the heat loss during ignition delay period, a non-reactive test, wherein O_2 in the test mixture is replaced with N_2, is conducted for each reactive case.

The compressed temperatures are calculated using the adiabatic core hypothesis,

$$\int_{T_i}^{T_c} \frac{\gamma}{\gamma - 1} \frac{dT}{T} = ln \frac{P_c}{P_i} \quad (1)$$

where the subscripts 'i' and 'c' indicate initial and compressed conditions, while γ is the ratio of specific heat of the gas mixture. The ideal gas law is applied over all of the experimental conditions including pre- and post-compression, and the specific heat of the gas is taken to be a function of the initial mixture composition as well as the individual specific heat of the gas constituents. The specific heat of each gas constituent is estimated from polynomial fits of published data, which are functions of temperature.

An energy balance approach [34] is used to calculate the heat release rates (HRR), and accumulated, or integrated heat release. The volumetric compression, and the accompanying heat loss and crevice flow processes are also incorporated into the analysis using measured non-reacting pressure traces. This can be expressed as,

$$HRR = \frac{\gamma}{\gamma - 1} \frac{dV}{dt} [P - P_{nr}] + \frac{1}{\gamma - 1} V \left[\frac{dP}{dt} - \left. \frac{dP}{dt} \right|_{nr} \right] - \frac{pV}{(\gamma - 1)^2} \left[\frac{d\gamma}{dt} - \left. \frac{d\gamma}{dt} \right|_{nr} \right] \quad (2)$$

where the subscript 'nr' indicates non-reacting condition. The gas temperature during the reactive tests is calculated using:

$$T \approx T_{nr} + x_b (LHV_{mix}/c_v) \quad (3)$$

where LHV_{mix} is the lower heating value of the mixture, c_v is the constant-volume specific heat of the mixture, and x_b is the fraction of fuel energy released, which can be deduced from $\int(HRR)dt/LHV_{mix}$.

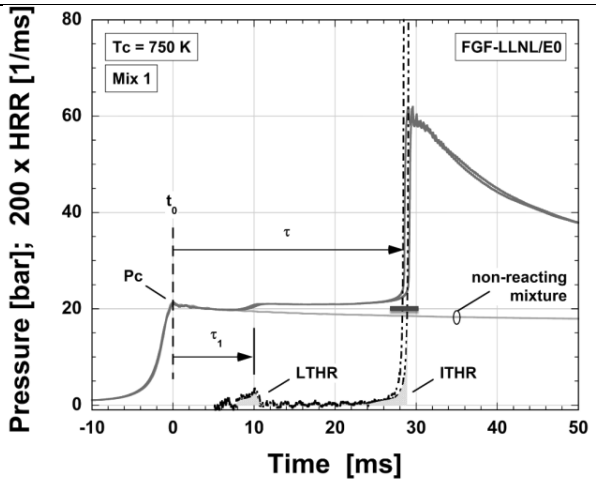

Figure 1. Representative experimental non-reacting and reacting pressure-time histories of FGF-LLNL/E0 (Mix 1) at Pc = 20 bar, Tc = 750 K with τ_1, τ, accumulated LTHR and ITHR identified. HRR is normalized by LHV_{mix}.

Figure 1 presents two representative reactive traces along with the associated non-reactive trace for 'neat' FGF-LLNL (FGF-LLNL/E0), where consistency between the two reactive shots, and alignment between the non-reactive and reactive traces prior to preliminary heat release events are excellent. Ignition delay times for first-stage (τ_1) and main ignition (τ) are also highlighted in Fig. 1, along with the LTHR and ITHR (intermediate temperature heat release) inferred from the accumulated HRR. The extent of LTHR is calculated as the integrated heat release from t_0 through the peak HRR at first-stage ignition (τ_1), up to the inflection point in HRR just before the start of ITHR (soITHR). Similarly, the extent of ITHR is calculated starting from the soITHR to the start of high temperature heat release (soHTHR). The soITHR and soHTHR are demarcated using $dHRR/dt = 0$ and $HRR{\sim}0.1/ms$, respectively, according to the definitions

from [35]. These thresholds are graphically illustrated in Fig. 6 below. Note that all heat release calculations presented in this work are normalized by the LHV of the test mixture, e.g., (J/mol/ms)/(J/mol).

Uncertainty analyses associated with ANL's tpRCM were presented in [32, 36], using a linear propagation approach similar to [37]. The uncertainty in computed Tc is estimated at 1.0-1.5%, due to instrumentation imprecision and procedural uncertainties associated with mixture preparation, and an uncertainty of $\pm$0.4 ms is estimated for each ignition delay measurement to account for the improper alignment with the non-reacting traces. Excellent consistency is achievable in the ANL tpRCM throughout the day, or week. This is demonstrated in Fig. S1, where a standard deviation of less than 2% is obtained from nearly twenty tests for an ethanol/air mixture at Tc = 862 K and Pc = 20 bar. Statistical (i.e., month-to-month) variability in τ however, can be on the order of $\pm$10%. It is important to recognize that quantifying the impact of Tc's uncertainty on τ is not straightforward due to the probability distribution of Tc within its uncertainty, interplay between Tc and other parameters given highly non-linear relations between Tc and τ, etc. Established frameworks of uncertainty quantification, such as [38, 39], can be adopted for such evaluation in the future, but is beyond the scope of this study. The uncertainty in calculation of heat release derives mainly from the use of single-zone formulation and the application of adiabatic core hypothesis, which do not account for exothermically-driven heat loss and gas transport to the piston crevice volumes. Measurement uncertainties in HRR are estimated at $\pm$7.4%, as discussed in [33, 36].

2.3. Test mixtures

Ethanol-blended fuels are prepared by adding 10, 20 and 30 liquid volume percent of ethanol (Sigma Aldrich, 200 proof, anhydrous, ≥99.5%) into 'neat' FGF-LLNL and FGF-KAUST (E0), designated at E10, E20 and E30. Each test fuel is studied in the RCM at two fuel loading conditions, one at diluted, stoichiometric conditions (15% O_2, ϕ =1 (Mixes 1 and 2 in Table 3)) and the other at undiluted, lean conditions (21% O_2, ϕ = 0.3 (Mixes 3 and 4 in Table 3)). The former is representative of boosted SI operation under elevated EGR (exhaust gas recirculation) scenarios, while the latter represents Homogeneous Charge Compression Ignition (HCCI) engine operation. Initial pressure, temperature and diluent composition in the reaction chamber are adjusted to achieve a range of compressed conditions. Table 3 summarizes the mixture compositions, and corresponding Tc ranges. Detailed information for individual tests can be found in the supplementary material.

Table 3. Summary of fuel loading conditions used in this study.

Mixture #	ϕ	O_2	N_2	Ar	Tc
Mix 1	1.0	~0.15	~0.84	0.00	< 830 K
Mix 2	1.0	~0.15	~0.21	~0.63	> 830 K
Mix 3	0.3	~0.21	~0.63	~0.16	< 890 K
Mix 4	0.3	~0.21	~0.31	~0.47	> 890 K

2.4. LLNL gasoline surrogate kinetic model

Building upon previous work at LLNL, including by Mehl et al. [40], an updated gasoline surrogate kinetic model is used in this study. The model is comprised of 1956 species and 10295 reactions and is provided in the Supplemental Material with a copy also hosted at the LLNL

combustion website (https://combustion.llnl.gov/mechanisms). In assembling the current model, additional identifiers (standard InChI, SMILES) for every species were assigned and the resulting "species dictionary" is available in the Supplemental Material. Readers are encouraged to find detailed descriptions of individual sub-models in the following references and often via the in-line comments within the model files.

A "core" C0~C4 sub-model developed by National University of Ireland, Galway (NUIG) [41] provides the foundation for the pyrolysis and oxidation of larger molecules. The chemistry of the compounds in this sub-model reflects contributions from new experiments and calculations from several preceding publications. This core chemistry sub-model has since been superseded by newer versions [42] and, while outside the scope of this study, future work at LLNL will seek to incorporate such improvements. Given the disagreement observed in [22] between the experimental measurements and model results at higher ethanol contents, the ethanol chemistry was further updated. Revisions based on the recent work of Zhang et al. [43] were incorporated, while H-atom abstraction reactions from ethanol by hydroperoxyl (HO_2) radical and O_2 addition reactions to the hydroxyethyl radicals have been rewritten following the work of Mittal et al. [44] and Miyoshi [45], respectively. Additional low-temperature reaction classes were updated following the work of Lizardo-Huerta et al. [46]. The updated kinetic sub-model for neat ethanol can be found in [47], and validations of the ethanol updates have been presented in Cheng et al. [48].

Reaction rate rules for paraffins are a foundational reference point for estimations of compounds with limited or no available literature. Bugler et al. [49], Zhang et al. [50], Mohamed et al. [51], and Fang et a. [52] critically reviewed and adopted literature calculations [53-56] of

low temperature (linear and branched) paraffin reaction rates following the widely accepted scheme of reaction classes described in the works by Curran et al. [57, 58]. Since then, these low temperature reaction rate rules have been successfully tested and refined against data for additional paraffins.

The 1-hexene sub-model, the only olefin in both FACE-F surrogates, is based on the work of Mehl et al. [59]. However, reaction rate constants and thermochemistry relevant to low temperature pathways were updated. The current sub-model performance was verified to meet or exceed that of with the current core sub-model [59]. Cyclopentane is also present in both FACE-F surrogates simulated in this work. Naphthenes are a class of compounds that may be present in commercial gasoline at levels near 10% liquid volume [60] but were not included in the 2011 model version. In the last several years a series of studies were undertaken to understand the chemistry of cyclopentane, with a new model most recently presented in Lokachari et al. [61], the smallest naphthenic compound considered for a gasoline surrogate.

Regarding aromatics, a systematic study of a series of alkyl substituted mono-aromatics (toluene, ortho-xylene, para-xylene, 1,2,4-trimethylbenzene, and 1,3,5-trimethylbenzene) and α-methylnapthalene [62] was used to develop reaction rate rules. This approach, which leveraged data spanning multiple fuels with similar moieties, has been a cornerstone of the recent updates introduced in LLNL-NUIG-KAUST models. Using data from several or more compounds in a class has strongly aided the development of more generally applicable reaction rate rules.

When available, care has been taken to utilize literature calculations for thermodynamic properties. In particular, efforts were taken to eliminate extreme outliers (greater than ~2 kcal/mol for enthalpies or ~2 cal/mol/K for entropies and heat capacities) from the

thermochemistry available in the Active Thermochemical Tables [63] and the work of Goldsmith et al. [64]. Additional updated species thermochemistry for which there was insufficient information in the literature were estimated using software implementations of group additivity such as THERM [65] and RMG [66]. A common issue related to thermochemistry is the stiffness of the ordinary differential equation system arising from the kinetic model. Although significant time-scale differences are intrinsic to kinetics, it has recently been highlighted how models with high levels of detail often include reaction rate constants with unphysical values at some conditions [67]. To avoid these issues, specific tools such as the LLNL developed Mech Checker [68] have been employed to check the timescales associated with the reaction rate constants used in the model and verify their physical soundness (e.g. against hard-sphere binary collision rates). Mech Checker can also correct discontinuities arising from ill fitted coefficients associated with the NASA 14-term polynomial representation [69] of a species' thermodynamic properties which can otherwise lead to additional computational stiffness.

While beyond the scope of work for this study, we also provide the transport properties necessary for simulating flames. Transport properties associated with this model were assigned from publications for respective sub-models when possible, e.g. Li et al. [41] for the C0~C4 sub-models, or estimated using established methods. Collisional diameter, σ, and energy well depth, ϵ/κ, transport parameters were estimated from the correlations of Dooley et al. [70]. Estimated polarizabilities were assigned using the correlation of Bosque and Sales [71]. No dipole moment and a unity rotational-collisional relaxation number were assumed for species with estimated properties. Nonlinearity was assumed for all estimated species unless deemed inappropriate.

Simulations of the RCM ignition delay times are completed using the LLNL-developed fast solver ZeroRK [72], including volume histories derived from non-reactive tests accounting for compression and heat loss.

3. RESULTS

3.1. Diluted, stoichiometric condition

Tests are conducted at two iso-baric conditions (Pc = 20 and 40 bar) covering Tc = 700–960 K. Figure 2 illustrates representative experimental and modeled pressure-time histories at Pc = 40 bar and Tc = 750 K for FGF-LLNL and FGF-KAUST at different levels of ethanol blending (E0–E30). The two repeated shots fired at each experimental condition show great consistency, with excellent agreement also exhibited with the non-reactive experiments prior to preliminary heat release events (i.e., LTHR, ITHR).

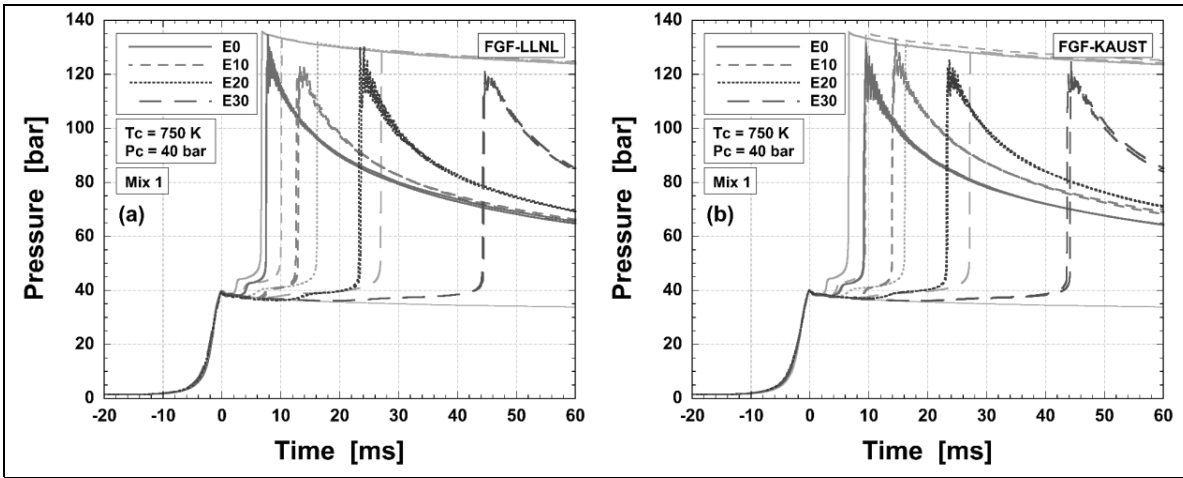

Figure 2. Measured and simulated pressure-time histories for (a) FGF-LLNL/E0–E30 and (b) FGF-KAUST/E0–E30 at Pc = 40 bar, Tc = 750 K, and the diluted/stoichiometric condition, with corresponding non-reactive results also included. Color lines indicate measurements, and gray lines are model results. Two-stage ignition behavior is observed, where first-stage and main ignition delay times, as defined in Fig. 1, can be determined; these are summarized in Fig. 5.

First, different behavior between the 'neat' surrogates can be observed in the experiments, where both surrogates exhibit two-stage ignition behavior, but FGF-LLNL/E0 displays somewhat greater main ignition reactivity than FGF-KAUST/E0. The higher reactivity of FGF-LLNL/E0 can be attributed to the compositional difference between the surrogates, e.g., n-heptane is contained in FGF-LLNL but not in FGF-KAUST, as discussed in detail later. The differences in 'neat' surrogate behavior observed here agree with previous studies [18, 21], where it was found that for surrogates with similar octane number, those with greater amounts of low-octane components, such as n-heptane are expected to display more substantial low-temperature reactivity.

Experimental results also show that ethanol consistently retards both τ_1 and τ for both surrogates, though it is seen that the magnitudes of perturbation do not linearly correspond to the volume of ethanol. Additionally, ethanol non-linearly suppresses the pressure rise at first-stage ignition, indicating a suppressing effect of ethanol on LTHR. Closer observation of Fig. 2 indicates difference between the surrogate/EtOH blends, where the FGF-LLNL/EtOH blends exhibit slightly higher reactivity than the FGF-KAUST/EtOH blends, with the difference diminishing towards higher levels of ethanol addition; these observations are detailed later in Figs. 6 and 7. This is mostly attributed to the slightly higher reactivity of the 'neat' FGF-LLNL compared to the 'neat' FGF-KAUST.

Simulated pressure-time histories are also presented in Fig. 2, where it is seen that the model tends to mute the differences between 'neat' FGF-LLNL and FGF-KAUST that are observed in the experiments, where nearly the same ignition characteristics are predicted. The global effects of ethanol blending are qualitatively captured by the model for both surrogates, including

retarded τ_1 and τ, and suppressed pressure rise during first-stage ignition. However, the reactivity of all test fuels is consistently over-predicted by the model, with quantitative disagreement in τ greatly increased as more ethanol is blended. The higher reactivity of 'neat' FGF-KAUST predicted by the model is consistent with previously reported JSR oxidation results for FGF-KAUST at diluted/stoichiometric conditions [21], wherein an earlier version of the chemical model used in this work also showed greater low-temperature reactivity than the experiments.

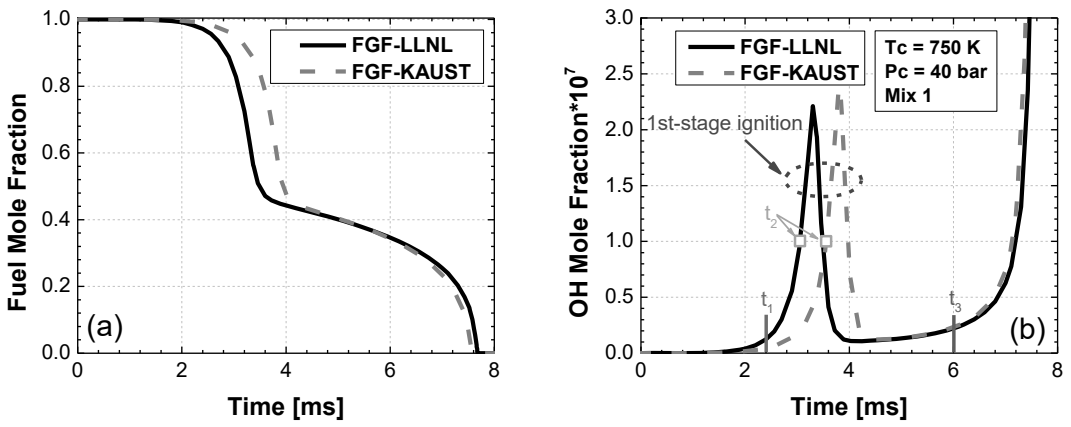

Figure 3. Simulated mole fraction of (a) 'neat' fuel and (b) OH, at Pc = 40 bar, Tc = 750 K, and the diluted/stoichiometric condition. Fuel mole fraction is normalized to 1.0, and ȮH mole fraction is multiplied by 10^7. t_1, t_2, and t_3 are defined.

Figure 3 next presents simulated fuel and ȮH mole profiles for the 'neat' surrogate blends at the same conditions as in Fig. 2, where differences in simulated oxidation processes are better clarified. Species mole profiles for the individual fuel components (five for FGF-LLNL, and seven for FGF-KAUST) are included in the Supplementary Material (Fig. S2). Despite similar predicted main-ignition reactivity, surrogate-to-surrogate differences in oxidation can be seen, where FGF-

LLNL decomposition is initiated earlier compared to FGF-KAUST with earlier onset of ȮH production.

To better elucidate the compositional effects on the 'neat' surrogate reactivity, flux analyses for ȮH are carried out using variable volume simulations at t_1 = 2.4 ms, times when $x_{OH} = 10^{-7}$ (identified as t_2), and t_3 = 6.0 ms. These timings are marked in Fig. 3b, where t_1 is the time where the 'neat' surrogates start to show differences in ȮH production, t_2 corresponds roughly to the times of maximum ȮH production rate, and t_3 is the time where nearly identical ȮH production is observed between the surrogates. Figure 4 presents the flux analysis results at t_1 and t_2 covering the top reactions and channels from different sub-chemistries, while the results at t_3 as well as fluxes of less important pathways at t_1 and t_2 are presented in the Supplementary Material. Different colors are used to illustrate different sub-chemistries, with black color employed for non-fuel-specific reactions. The numbers shown are in percent, which are computed as the ratio of the rate of consumption (or production) for that pathway to the total rate of consumption (or production).

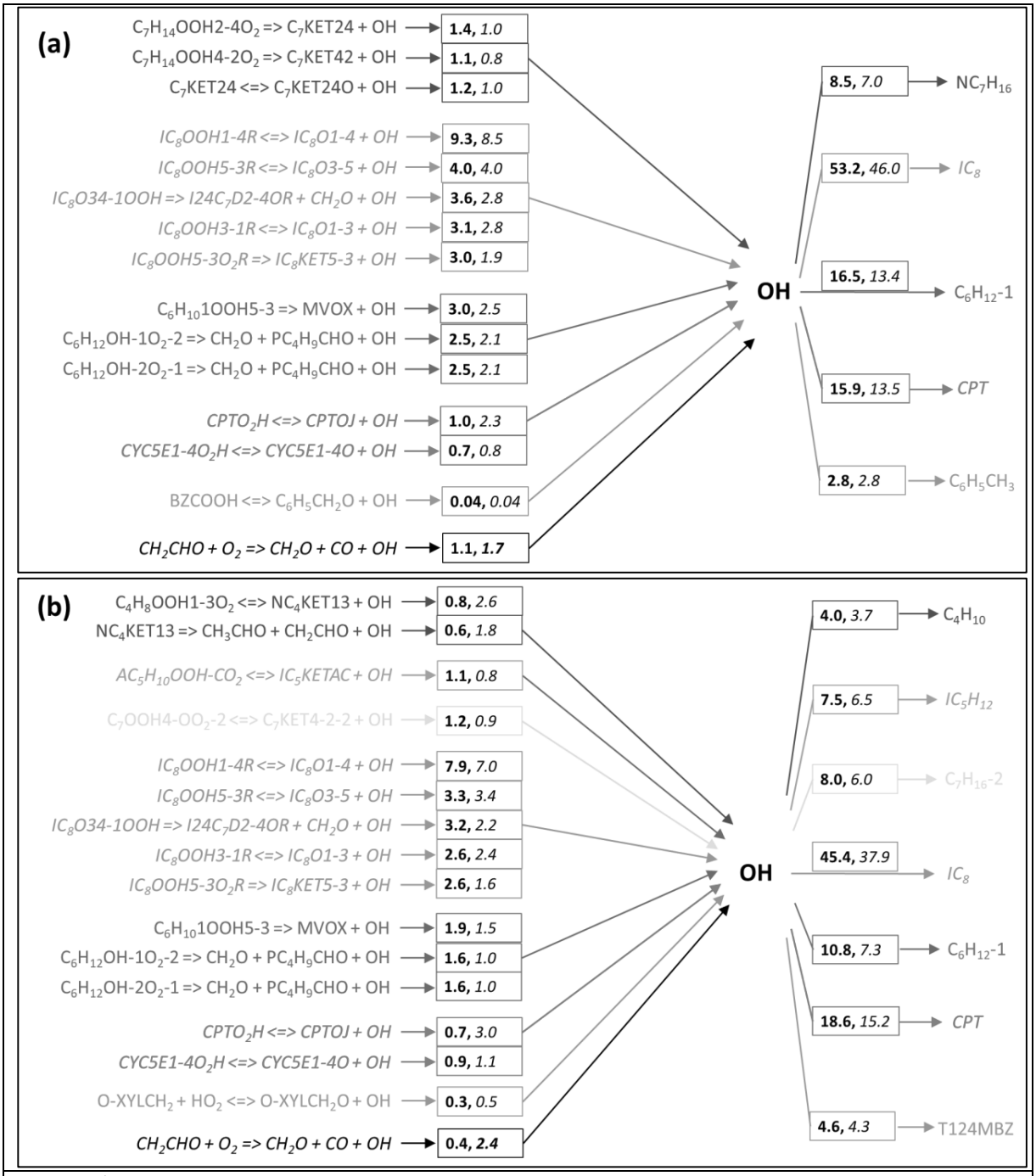

Figure 4. ȮH flux analysis for (a) FGF-LLNL/E0 and (b) FGF-KAUST/E0 at Pc = 40 bar, Tc = 750 K, and the diluted/stoichiometric condition, same as with Fig. 3. Numbers represent the percentage of ȮH consumed or produced by that pathway. Bold numbers represent the flux at t_1 = 2.4 ms after EOC; italic numbers represent the flux at roughly the max rate of production during first-stage ignition, i.e., $x_{OH} = 10^{-7}$ in Fig. 3a. Different colors represent the top ȮH producing reactions from the chemistry of each surrogate component, while black color represents the non-fuel-specific reactions. The participating species can be identified in the species dictionary in the Supplementary Material. Numbers shown for each surrogate component are in percent, which are computed as the ratio of the rate of consumption (or production) for that pathway to the total rate of consumption (or production).

For both surrogates, at t_1 ȮH is mainly produced from iso-octane and 1-hexene chemistry via decomposition of QOOH and OOQOOH radicals, due primarily to their dominant concentrations in the surrogate blends, while contributions from n-heptane chemistry are also significant for FGF-LLNL/E0. Nearly all produced ȮH is consumed via H-atom abstraction reactions from fuel molecules, with the contribution of each surrogate component being roughly proportional to its concentration, except for the low-reactivity components, i.e., toluene for FGF-LLNL/E0 and 1,2,4-trimethylbenzene for FGF-KAUST/E0. The higher ȮH production for FGF-LLNL/E0 at t_1 can be attributed to several reasons. First, 8.5% of produced ȮH is consumed by n-heptane. The produced n-heptyl radicals lead to formation of ȮH and keto-hydroperoxides that further decompose to produce additional ȮH. Such pathways are major contributors to ȮH production at t_1, as seen in Fig. 4a, while for FGF-KAUST/E0 (Fig. 4b), the n-alkane counterpart, i.e., n-butane, accounts for 4% of ȮH consumption but has minor contributions to ȮH production. 2-methyl hexane, which has a sizable alkane backbone and is in FGF-KAUST/E0, is seen to also not be as important as n-heptane. Second, the highly reactive ȮH produced from n-heptane chemistry are able to abstract H-atom from the less reactive hydrocarbons, e.g., iso-octane and 1-hexene, thereby initiating their low-temperature oxidation process at an earlier point to further facilitate ȮH production. This is elaborated in Fig. S2a, where n-heptane displays the earliest start of oxidation process among all FGF-LLNL components, and this leads to earlier and faster consumption of iso-octane and 1-hexene compared to those for FGF-KAUST.

At t_2, the contributions to ȮH production from most pathways are somewhat weakened, while those from cyclopentane chemistry, n-butane chemistry and pertaining to small

intermediates are enhanced. Particularly, there is a considerable increase in n-butane contribution for FGF-KAUST/E0, e.g., via decomposition of n-butyl hydroperoxides and keto-hydroperoxides, as highlighted in Fig. 4b. Decomposition of n-butyl keto-hydroperoxides yields CH_2CHO, which further promotes ȮH production via $CH_2CHO+O_2<=>CH_2O+CO+OH$, resulting in a higher increase in the flux of this reaction for FGF-KAUST/E0 than for FGF-LLNL/E0. Additionally, a relatively higher increase of cyclopentane contribution is shown for FGF-KAUST/E0 (e.g., contribution of $CPTO_2H<=>CPTOJ+OH$ increases from 0.7% to 3.0% for FGF-KAUST/E0 while only from 1.1% to 2.3% for FGF-LLNL/E0), likely due to the slightly higher concentration of cyclopentane in FGF-KAUST (Table 1). The increased ȮH production from these pathways compensates the deficit in ȮH production for FGF-KAUST/E0 at t_1, eventually leading to the same ȮH production as FGF-LLNL/E0 at t_2. The importance of these pathways in controlling the initial fuel reactivity during first-stage ignition suggests that improvements can be made for the relevant chemistry to reduce the discrepancies between the experiments and model results, and to better replicate the reactivity differences between the 'neat' surrogates.

At t_3, compositional effects are less profound since ȮH production becomes less dependent on fuel-specific reactions, but is instead controlled by small radical reactions such as H_2O_2 decomposition, as shown in the Supplementary Material. The differences between the 'neat' surrogates are therefore minimized at this time.

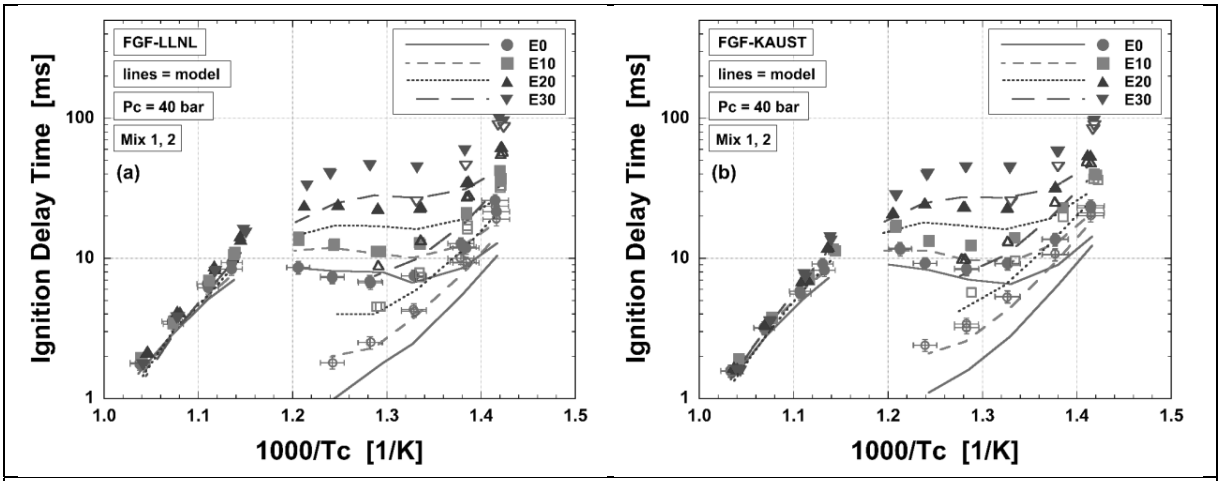

Figure 5. Experimental and modeled ignition delay times of (a) FGF-LLNL and (b) FGF-KAUST with 0–30% vol./vol. ethanol blended at Pc = 40 bar, phi = 1, and 15% O_2. Symbols indicate experiment (open – first-stage; closes – main ignition) and lines are model results. Representative experimental uncertainties are demonstrated for (a) FGF-LLNL/E0 and (b) FGF-KAUST/E0.

Figure 5 presents the measured and simulated first-stage and main ignition delay times for the 0–30% vol./vol. blends of FGF-LLNL/EtOH and FGF-KAUST/EtOH as functions of inverse temperature at Pc = 40 bar and Tc = 700 to 1000 K. The results at Pc = 20 bar are presented in Fig. S4 in the Supplementary Material. Measurements for 'neat' surrogates demonstrate distinct low-temperature, NTC (negative temperature coefficient), and intermediate-temperature behavior [73]. Within the low-temperature/NTC regime (700 K < Tc < 860 K), two-stage ignition behavior is evident, where the first-stage ignition reactivity increases monotonically with temperature, while within the intermediate-temperature regime (860 K < Tc < 1000 K), first-stage ignition is completely absent. As previously seen in Fig. 2, differences between FGF-LLNL/E0 and FGF-KAUST/E0 are also observed in Fig. 5, where FGF-LLNL/E0 exhibits less pronounced NTC behavior, and higher reactivity within the low-temperature/NTC regime but slightly lower reactivity within the intermediate-temperature regime [19]. Also seen from Fig. 5 is the earlier first-stage ignition for FGF-LLNL/E0 than for FGF-KAUST/E0.

Ethanol blending effects are evident in Fig. 5, with similar trends seen in the experimental data for both surrogates, and qualitatively consistent with previous measurements with FACE-F/E0–E30 at similar conditions in the same RCM [22]. Due to the different blending behaviors observed across the two temperature regimes, discussions of ethanol effects are segregated into two parts: low-temperature/NTC (700 K < Tc < 860 K) and intermediate-temperature (860 K < Tc < 1000 K). In the low-temperature/NTC regime, ethanol strongly suppresses fuel reactivity for both surrogates, yielding increased τ_1 and τ, with first-stage ignition being suppressed for higher amounts of ethanol at higher temperatures, resulting in single-stage autoignition behavior. This can be seen in Fig. 5 at Tc = 780 K, where first-stage ignition is no longer observed with 30% vol. ethanol added. The suppressing effect of ethanol on low-temperature reactivity can be attributed to the unique oxidation pathway of ethanol at low temperatures, where ethanol scavenges ȮH radicals via H-atom abstraction from the α-site forming 1-hydroxyethyl followed by reaction with O_2 [25], leading to the production of aldehydes and HO_2 radicals that are stable at low temperatures. Blending ethanol also causes a shift in ȮH consumption favoring the H-atom abstraction from ethanol over other surrogate components, which aids the progression towards ȮH termination that would otherwise lead towards ȮH branching [22]. Also discernable are the different quantitative responses between the surrogates to ethanol addition, particularly within the NTC regime, where greater perturbations in τ_1 and τ are observed for FGF-LLNL/E0-E30 than for FGF-KAUST/E0-E30. This behavior is more clearly presented in Figs. 6 and 7, and could suggest that ethanol has higher synergistic blending behavior with FGF-LLNL than FGF-KAUST for the E10 and E20 blends. Consistent with Fig. 2, adding ethanol diminishes the reactivity difference

between the two surrogates across the temperature range studied, due in part to ethanol becoming the most abundant component in the blends.

In the intermediate-temperature regime, all test fuels exhibit markedly Arrhenius behavior, and the influence of ethanol addition is much weaker, where ethanol slightly increases fuel reactivity. This is contrary to the trend observed at low temperatures. This trend has been explained by previous work [22], wherein ethanol was found to facilitate H_2O_2 formation via $C_2H_5OH+HO_2=SC_2H_4OH+H_2O_2$. At intermediate temperatures, the produced H_2O_2 radicals subsequently decompose to ȮH, leading to chain branching, and hence increased autoignition reactivity. Unlike the trends at low temperatures, the qualitative difference in fuel reactivity between FGF-LLNL/E0–E30 and FGF-KAUST/E0–E30 is consistent regardless of the amount of ethanol added, where FGF-KAUST/E10–E30 are more reactive, though the differences are minor. It should be noted that the high paraffin and low aromatic composition of FACE-F and its surrogates can lead to different response to ethanol in comparison to some commercial gasolines [29]. However, this does not affect the analyses in this work since comparisons are made between FACE-F and its surrogates.

The model results shown in Fig. 5 captures the qualitative trends of the experimental measurements for both 'neat' surrogates, including the two-stage and single-stage behaviors of the 'neat' surrogates across the wide span of temperature, and the suppressing effects of ethanol on both first-stage and main ignition over this span. However, the model displays greater first-stage and main ignition reactivity than the experiments except for the main ignition reactivity of FGF-LLNL/E0 at Tc = 770–860 K (Fig. 5a), with better agreements observed in the intermediate-temperature regime than in the low-temperature/NTC regime. Also, the model fails to capture

the main ignition reactivity difference between the neat surrogates within the low-temperature/NTC region. Specifically, the model predicts nearly the same reactivity for the neat surrogates at the lowest temperature studied, while higher reactivity for FGF-KAUST than for FGF-LLNL at the middle range of the NTC region, which is contrary to the experiments, though much of the observed quantitative differences between model and experimental results can be obscured by the experimental uncertainties. Nevertheless, the model captures the neat surrogate-to-surrogate difference in first-stage ignition reactivity, which is consistent with Fig. 3b. It should be noted that the insufficiency of the model in capturing the surrogate-to-surrogate differences is not due to the uncertainties in blending the surrogates, which will only lead to small data fluctuation instead of the consistent and large reactivity difference between the neat surrogates as seen in Fig. 5. Overall, the model captures better the NTC behavior for FGF-LLNL/E0 than for FGF-KAUST/E0. In the low-temperature/NTC regime, the model under-predicts the influences of ethanol addition for both surrogates, with the level of agreement deteriorating with higher extents of ethanol blending for both first-stage and main ignition reactivity, similar to that observed in Fig. 2.

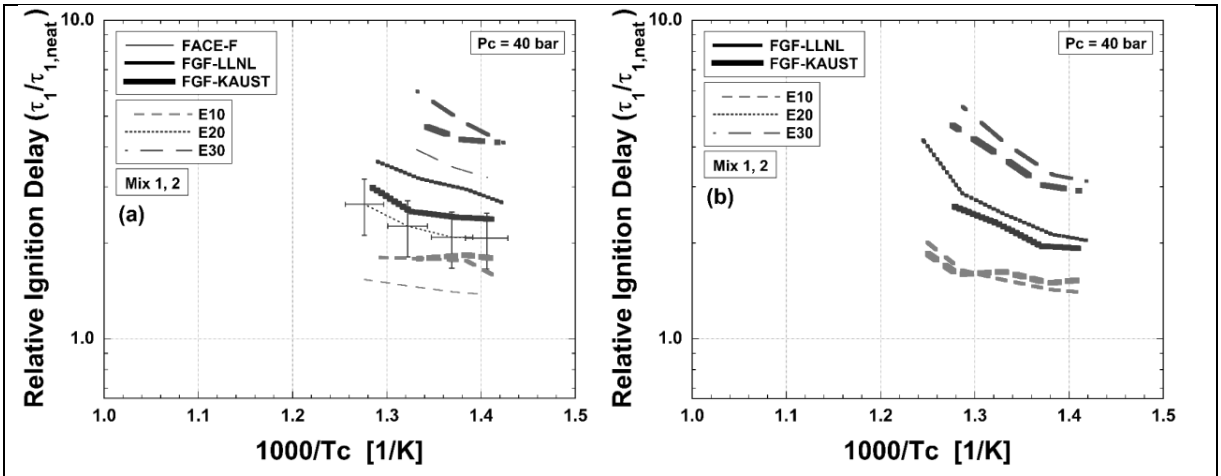

Figure 6. Experimental (a) and modeled (b) relative first-stage ignition delay times (τ^*) with different amounts of ethanol blended at Pc = 40 bar, phi = 1, and 15% O_2, presented as functions of inverse temperature. τ_1^* is the ratio to the 'neat' fuel, i.e., $\tau_1^* = \tau_1/\tau_{1,neat}$. Experimental data for FACE-F/E0–E30 blends are taken from [22].

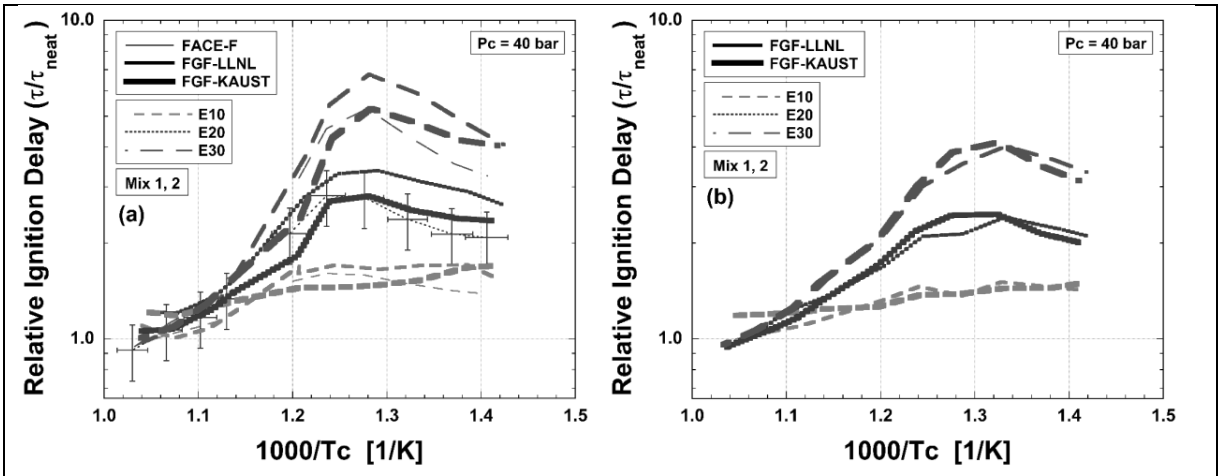

Figure 7. Experimental (a) and modeled (b) relative main ignition delay times (τ^*) with different amounts of ethanol blended at Pc = 40 bar, phi = 1, and 15% O_2, presented as functions of inverse temperature. τ^* is the ratio to the 'neat' fuel, i.e., $\tau^* = \tau/\tau_{neat}$. Experimental data for FACE-F/E0–E30 blends are taken from [22].

To better illustrate the perturbative characteristics of ethanol blending and differences in surrogate response to ethanol, relative first-stage and main ignition delay times for the dataset are presented in Figs. 6 and 7, respectively, as functions of inverse temperature. Relative times are defined as the ratio of the ignition delay time of the ethanol-blended fuel to that of the

corresponding ethanol-free, or 'neat' fuel, i.e., $\tau_1^* = \tau_1/\tau_{1,neat}$ and $\tau^* = \tau/\tau_{neat}$. Relative times below 1.0 indicate that ethanol promotes reactivity, while those above 1.0 indicate an inhibiting effect. The experimental data for FACE-F/EtOH blends [22] are also presented in Fig. 6a and 7a for direct comparison with the surrogate/EtOH blends.

Immediately evident in Fig. 6a are the strong, non-linear suppressing effects of ethanol on first-stage ignition reactivity for both FGF-LLNL and FGF-KAUST, where the ranking appears as FGF-LLNL > FGF-KAUST > FACE-F. The suppressing effects exhibit positive temperature dependence where the relative influence monotonically increases with Tc (except for the experimental FGF-KAUST/E10 which has little temperature dependence). The trends of τ* are more complicated, as seen in Fig. 7a, due to the significant suppressing effects at low-temperature/NTC conditions and slight promoting effects at the highest temperatures explored in this work. Within the low-temperature/NTC regime, the reactivity suppressing effects between the surrogates can be ranked as FGF-LLNL > FGF-KAUST ~ FACE-F, with peak suppression occurring near Tc = 780 K for E30 blends.

The model results shown in Fig. 6b and 7b qualitatively reproduce the non-linear suppressing effects and the temperature dependence observed in the experiments. On the relative basis, it is clear that the model under-predicts the suppressing effects of ethanol while the surrogate-to-surrogate differences experimentally observed between FGF-LLNL/EtOH and FGF-KAUST/EtOH are also not captured. The latter may be due to the inability of the model to replicate the compositional effects of the 'neat' surrogate, as well as the intermolecular interactions between ethanol and fuel constituent decomposition/oxidation products.

As discussed with Figs. 2 and 5, the model predicts similar times of first-stage ignition for the 'neat' surrogates where about ~15% longer times are seen for FGF-KAUST/E0 compared to FGF-LLNL/E0 across the low-temperature/NTC conditions. The experimental measurements though indicate different temperature dependencies for the two surrogates, with the fuels having nearly the same first-stage ignition reactivity at 700 K, but FGF-KAUST/E0 becomes progressively slower at higher temperatures, e.g., ~35% longer at 800 K, as shown in Fig. 5. Discrepancies are also observed for main ignition times where the model indicates similar reactivity for the two 'neat' fuels (±5%) across both temperature regimes, while the measurements show that FGF-KAUST/E0 is progressively slower than FGF-LLNL/E0 by 0–30% from 700 to 830 K, but about 10% faster at higher temperatures, e.g., 880–960 K. Such differences in base ignition delay times used to calculate relative times can cause the quantitative differences seen in Figs. 6 and 7. For instance, Fig. 2 shows smaller experimental ignition delay times (both first-stage and main) for 'neat' FGF-LLNL compared to 'neat' FGF-KAUST at Tc = 750 K, with such reactivity differences being significantly diminished as ethanol is blended. As a result, the relative times are expected to be higher for FGF-LLNL than for FGF-KAUST at this temperature, as can be seen in Figs. 6a (except for E10) and 7a. The simulated relative times for the surrogates are similar at this temperature (Figs. 6b and 7b) since the model predicts similar first-stage and nearly identical main ignition reactivity for the 'neat' surrogates.

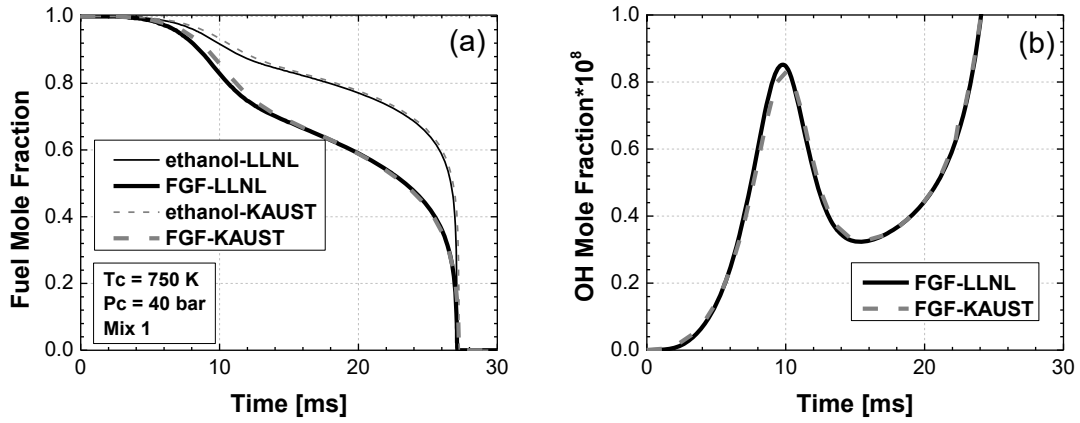

Figure 8. Simulated mole fractions of (a) 'neat' surrogate and ethanol, and (b) ȮH for FGF-LLNL/E30 and FGF-KAUST/E30 blends, at Pc = 40 bar, Tc = 750 K, and the diluted/stoichiometric condition. Fuel mole fractions are normalized to 1.0, and ȮH mole fraction is multiplied by 10^8.

To better understand the differences in perturbative influence between the two surrogates, Fig. 8 presents simulated fuel and ȮH profiles for ethanol and the hydrocarbon constituents of the surrogate blends at the 30% vol. blend level where the ethanol and 'neat' components are shown separately. Again, the fuel mole fractions in Fig. 8a are normalized against the initial concentrations, and the same conditions as in Figs. 2 and 3 are used. Profiles for the individual constituents of the 'neat' fuels are presented in Fig. S3 in the Supplementary Material. Figure 8a shows that at 30% vol. EtOH blending, FGF-LLNL becomes similarly reactive to FGF-KAUST during first-stage ignition, resulting in nearly the same fuel consumption rates. The ȮH profiles seen in Fig. 8b also indicate that the differences in first-stage ignition reactivity observed in Fig. 3 (i.e., FGF-LLNL/E0 produces ȮH radicals earlier than FGF-KAUST/E0) are greatly muted. Previous work [22] found that at low temperatures, ethanol interferes with FGF-LLNL oxidation primarily by competing with other fuel components, particularly iso-octane, in ȮH consumption, where H-atom abstraction from ethanol to form α-hydroxyl ethanol radical (SC_2H_4OH) is more

favored over those from other fuel constituents. The earlier start of first-stage ignition reactivity for FGF-LLNL/E0 (c.f. Fig. 3) is mainly due to the ȮH radicals produced from n-heptane initiating oxidation of other components, such as iso-octane and 1-hexene. However, with ethanol blending, many ȮH radicals produced from n-heptane chemistry are prevented from abstracting H-atoms from iso-octane or 1-hexene molecules, and are instead consumed by ethanol, leading to greater yield of less reactive intermediates such as acetaldehyde and HO_2. These shifts in ȮH consumption towards ȮH radical scavenging weakens the ignition promoting effects of n-heptane, leading to reduced first-stage ignition reactivity for FGF-LLNL that eventually becomes similar to FGF-KAUST.

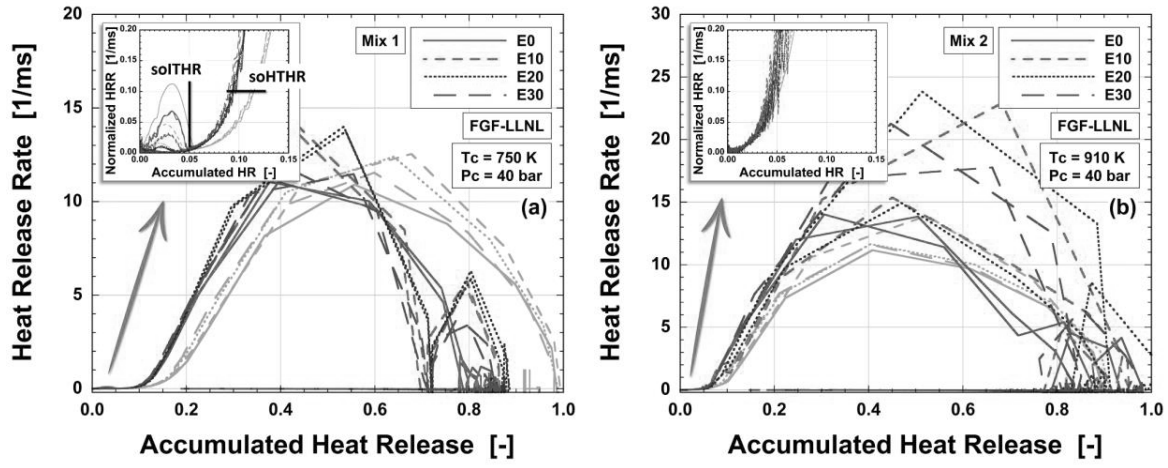

Figure 9. Calculated, normalized experimental and modeled heat release rates presented as functions of accumulated heat release for FGF-LLNL/E0–E30 blends at Pc = 40 bar, phi = 1, 15% O2, and (a) Tc = 750 K and (b) 910 K. Insets depict preliminary exothermicity with LTHR and ITHR demarcations identified, i.e., soITHR and soHTHR, respectively. Color lines are experimental results; gray lines are model results. Each mixture has two experimental curves that represent two reactive tests performed. The insets are provided as Supplementary Material (Fig. S5) to allow better interpretation of LTHR and ITHR between experiments and simulations.

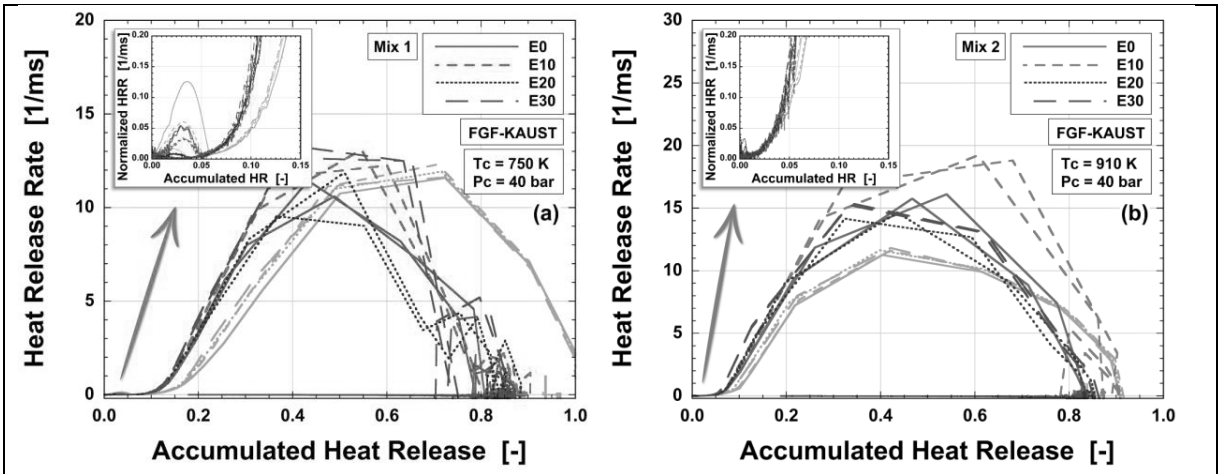

Figure 10. Calculated, normalized experimental and modeled heat release rates presented as functions of accumulated heat release for FGF-KAUST/E0–E30 blends at Pc = 40 bar, phi = 1, 15% O2, and (a) Tc = 750 K and (b) 910 K. Insets depict preliminary exothermicity with LTHR and ITHR demarcations identified, i.e., soITHR and soHTHR, respectively. Color lines are experimental results; gray lines are model results. Each mixture has two experimental curves that represent two reactive tests performed. The insets are provided as Supplementary Material (Fig. S6) to allow better interpretation of LTHR and ITHR between experiments and simulations.

To identify the effects of ethanol blending on the exothermic behavior of the two FACE-F surrogates, the LHV-normalized heat release rates for FGF-LLNL/E0–E30 and FGF-KAUST/E0–E30 are presented in Figs. 9 and 10, respectively, as functions of accumulated heat release. The insets in Fig. 9–10 are included in the Supplementary Material (Fig. S5–S6) as separate figures to allow better tracking of comparisons between experiments and simulations for LTHR and ITHR. Two temperature conditions, i.e., Tc = 750 and 910 K, are shown here to indicate the behavior within the low-/NTC and intermediate-temperature regimes, respectively. The HRR trajectories start at the origin and evolve from left to right. Preliminary exothermicity, including LTHR and ITHR whenever applicable, can be seen at the lower left corner of the plot, where these are enlarged in the insets. Detailed discussion of the exothermic features can be found in [22, 33, 36]. The experimental accumulated heat release being lower than 1.0 is due to the assumptions made in computing HRR, where the exothermically-induced energy losses, e.g., enhanced heat transfer

to the walls and gas transfer to the crevice, are not fully taken into account in the calculation. The model is able to reach 1.0 since the reactive test is assumed to have the same post-compression heat loss characteristics as the corresponding non-reactive test.

For the experimental results at Tc = 750 K (Figs. 9a and 10a), it is evident that there are many qualitative similarities between the two 'neat' surrogates including the existence of, and similar magnitudes for preliminary exothermicity. The inset in Fig. 9a demarcates the extents of LTHR and ITHR where the transitions to intermediate- and high-temperature heat release are designated as soITHR and soHTHR, respectively. Additionally, peak HTHR rates during the process appear to occur at 40–60% of the lower heating value of the mixture, while at the tail end of exothermicity, i.e., at the highest temperature/pressure conditions, the process appears to proceed at slower rates than during the main heat release. This last feature could be a chemical kinetic process, or just an artifact of physical effects in the reaction chamber, such as the transfer of gas forced into dead volumes within the test chamber [33]. Quantitative differences between the preliminary exothermic behavior of FGF-LLNL/E0 and FGF-KAUST/E0 can also be seen, where FGF-LLNL/E0 displays a slightly faster transition to LTHR and slightly higher magnitudes of heat release rate during LTHR. These trends are consistent with the pressure-time histories shown in Fig. 2, where faster pressure rise is seen during first-stage ignition for FGF-LLNL/E0.

There are many similarities in the ethanol blending effects that can be seen in Figs. 9a and 10a, where adding ethanol reduces both the rates and extents of LTHR, while at this pressure (P_c), ethanol blending has almost no impact on the total preliminary heat release, i.e., accumulated LTHR+ITHR. LTHR+ITHR can be determined from the accumulated heat release at soHTHR, as defined by $HRR \sim 0.1/ms$ in Section 2.2.4. This is because the chemistry governing

the transition to HTHR is similar for all of the blended fuels, e.g., the fluxes at t3 in the Supplementary Material, and requires similar build ups of associated radical concentrations and temperature.

At Tc = 910 K (Figs. 9b and 10b), there is no LTHR for either surrogate, and therefore FGF-LLNL/E0 and FGF-KAUST/E0 display negligible differences in their preliminary HRR characteristics, indicating that the compositional effects between the 'neat' surrogates are more relevant to low-temperature reactivity. Furthermore, the influence of ethanol blending on ITHR at this temperature is negligible and consistent between the two surrogates, where the total preliminary heat release only accounts for about 5% of total fuel energy for all the fuel blends.

By reviewing the model results presented in Figs. 9 and 10, it is evident that the general/qualitative trends observed in the experimental measurements (e.g., temperature effects and ethanol blending effects) are replicated by the model, but there are some quantitative discrepancies. Particularly, the model does not capture the neat surrogate-to-surrogate difference at Tc = 750 K. At this temperature, the peak HRR during LTHR is lower for FGF-LLNL/E0 than for FGF-KAUST/E0, which is contrary to the experiments, but consistent with the results shown in Fig. 3b, where FGF-LLNL/E0 exhibits an earlier evolution of OH production but a lower magnitude of peak OH concentration during first-stage ignition. Additionally, both surrogates exhibit behavior that is different from the experimental measurements at the tail end of exothermicity, which requires more investigation to clarify. At Tc = 910 K, the model shows better correspondence with the experiments for both surrogates, while there appears to be little difference between the heat release behaviors of FGF-LLNL/E0–E30 and FGF-KAUST/E0–E30.

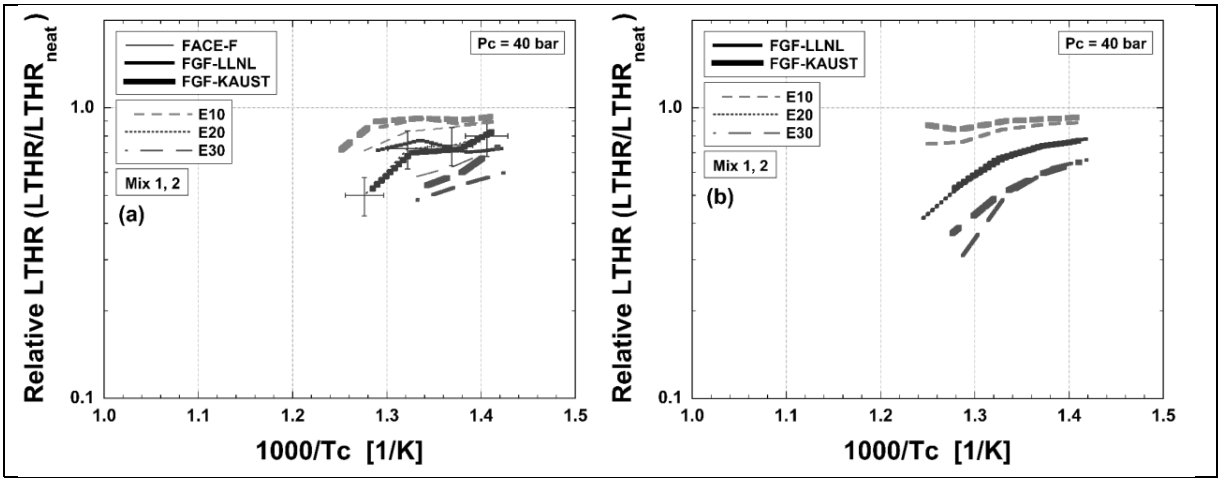

Figure 11. Calculated, normalized experimental (a) and modeled (b) relative LTHR ($LTHR^*$) with different amounts of ethanol blended at Pc = 40 bar, phi = 1, and 15% O_2, presented as functions of inverse temperature. $LTHR^*$ is defined as the ratio to the 'neat' fuel, i.e., $LTHR^* = LTHR/LTHR_{neat}$. Experimental data for FACE-F/E0–E30 blends are taken from [22].

Figure 11 next presents the relative accumulated LTHR as functions of inverse temperature for the experiment and model results to quantify the impact of ethanol blending on preliminary exothermic behavior for the two surrogates. The relative accumulated LTHR is defined as $LTHR/LTHR_{neat}$, where $LTHR$ and $LTHR_{neat}$ are the accumulated LTHR of the ethanol-blended fuel and of the 'neat' fuel, respectively. Analogous to the relative ignition times, values above 1.0 indicate that ethanol promotes LTHR, while values below 1.0 indicate an inhibiting effect. As with Figs. 6a and 7a, the results for FACE-F/E0–E30 reported in [22] are included in Fig. 8a for direct comparison.

As with the relative first-stage ignition delay times shown in Fig. 6a, it can be seen that ethanol blending also significantly suppresses the extents of LTHR for both surrogates, with the degree of suppression somewhat increasing with Tc. The suppressing effects are slightly greater for FGF-LLNL/EtOH than for FGF-KAUST/EtOH for E30, though experimental uncertainties in the LTHR calculations could obscure the differences. The suppressing effects are expected since FGF-

LLNL/E0 displays slightly higher extents of LTHR than FGF-KAUST/E0 (as seen in Fig. 9a and 10a) due to the presence of n-heptane which initiates rapid OH branching, and this is significantly suppressed by ethanol blending. Nevertheless, the behavior of both surrogates appears fairly close to that of FACE-F, though the progression from E10 to E30 is smaller in magnitude for the full boiling-range fuels than for the two surrogate blends. The trends observed here are similar to those seen in Fig. 6a and 7a, indicating a strong correlation between low-temperature ignition reactivity, both first-stage and main ignition reactivity, and LTHR.

The model (Fig. 11b) reasonably captures the trends in relative LTHR for the test fuels, though there are discrepancies compared to the experimental measurements. In particular, the model shows slightly greater suppressing effects than observed experiments. This may be due to the over-predicted extents of LTHR for the 'neat' surrogates, as seen in Figs. 9a and 10a. The model also does not appear to capture the surrogate-to-surrogate differences in LTHR for E20 and E30 where nearly identical magnitudes of ethanol perturbation are found, particularly at low temperatures. This is again consistent with observations for the first-stage and main ignition reactivity shown in Fig. 6b and 7b, and may be attributed to the inadequacy of the model in capturing some of the compositional effects between the neat surrogates.

3.2. Undiluted, lean condition

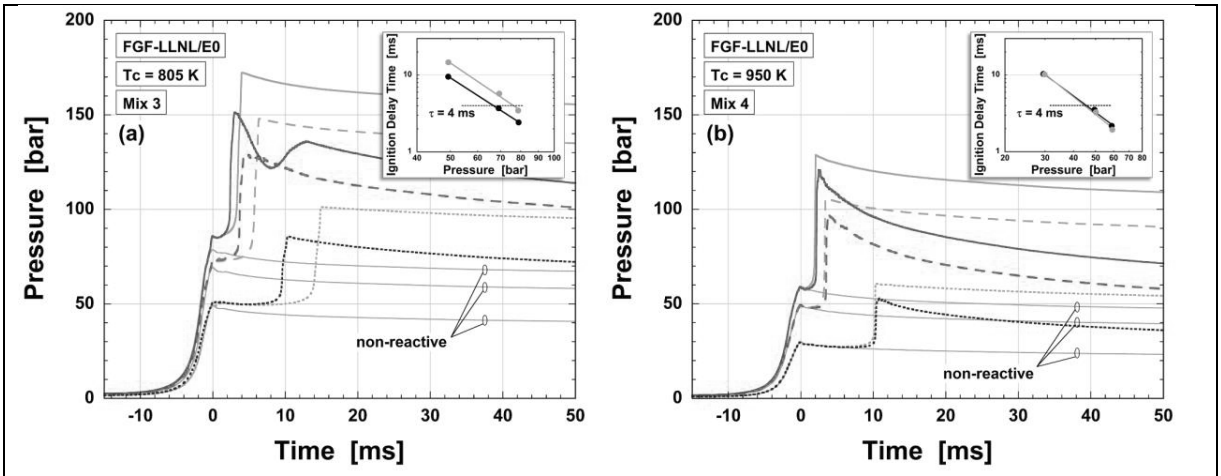

Figure 12. Measured and simulated pressure-time histories for FGF-LLNL/E0 at the undiluted/lean condition covering different compressed pressures, and (a) Tc = 805 K and (b) 950 K, with corresponding non-reactive results also included. Some exothermicity is evident before the end of compression in (b), as discussed in the text. Insets illustrate test campaign to identify pressure condition at τ = 4 ms. Color lines are experimental results; gray lines are model results.

Tests are conducted at the undiluted, lean fuel loading covering a range of pressure and temperature (Pc = 15–100 bar ; Tc = 780–1000 K) where the intent is to access conditions yielding autoignition times relevant to HCCI engine operation (e.g., τ = 2–10 ms [22, 36]). Figure 12 presents representative experimental and modeled pressure-time histories for FGF-LLNL/E0 at Tc = 805 K and 950 K, with the corresponding non-reactive histories shown to highlight the good consistency in the tests. The sweep of pressures at the two Tc conditions, as shown in the insets, illustrates how τ can be manipulated to a desired combustion phasing. Specifically, at a fixed Ti/Tc, Pc is swept to alter τ until it covers the desired range. In Fig. 12a, it can be seen that at the highest pressures (e.g., Pc = 70+ bar), there is significant reactivity during piston compression with LTHR initiated just before t_0. The experimental protocol used in these tests is robust however, even under this scenario since there is excellent agreement between the non-reactive and reactive tests during most of the piston compression process. The compressed conditions

are therefore identified based on non-reactive tests, while τ_1 could be earlier than t_0, and thus impossible to be represented on an Arrhenius diagram, or through a relative basis (e.g., Figs. 5–7). It should be noted that the simulation protocol is also robust since the boundary conditions needed are generated via each of the non-reactive tests. Also evident in Fig. 12a is the presence of piston rebound at the highest pressures, e.g., Pc = 85 bar, where there is a pressure fluctuation shortly after the peak pressure. This is due to insufficient time available to transfer hydraulic fluid from the tpRCM's accumulator to engage the hydraulic lock. This feature does not affect the determination of τ, or significantly affect the heat release analyses. The slight effects on HRR and aHR are seen as an apparent loss in fuel energy of approximately 2–4%, as discussed in [36].

The simulated pressure-time histories show fairly good correspondence with measurements, including the evolution of LTHR in Fig. 12a at the highest pressure conditions, as well as the shifts in ignition reactivity due to pressure. Excellent agreement is observed at Tc = 950 K. At Tc = 805 K, the model under-predicts ignition reactivity, a discrepancy somewhat contrary to those observed at diluted/stoichiometric condition where the model is more reactive at the low-temperature/NTC conditions.

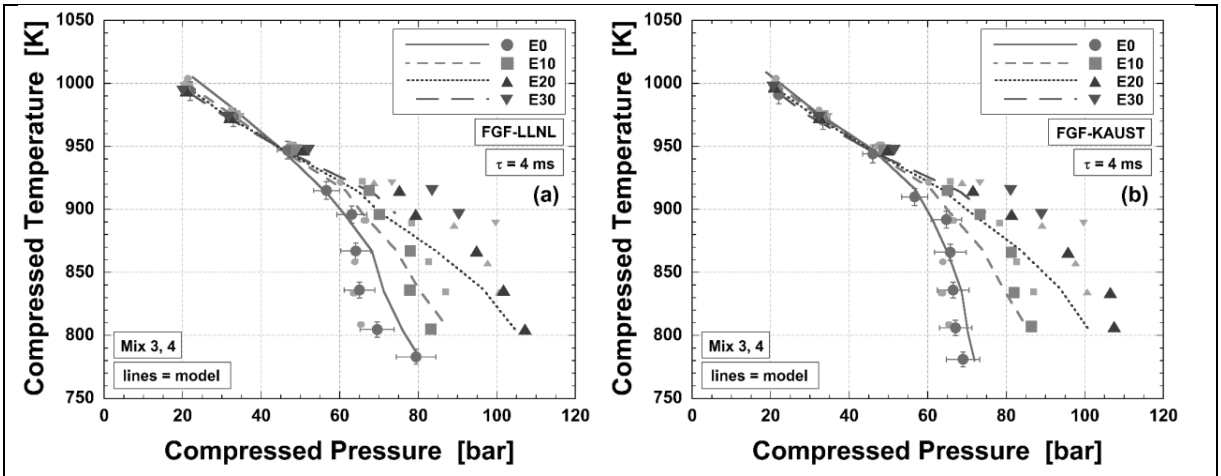

Figure 13. Experimental and modeled isopleths of τ = 4 ms for FGF-LLNL (a) and FGF-KAUST (b) with 0–30% vol./vol. ethanol blended covering a range of compressed temperature and pressure. Representative experimental uncertainties are shown for the two 'neat' surrogates. Experimental results for FACE-F/E0–E30 reported in [22] are also included for comparison. Symbols are experimental results (color – surrogate/E0–E30; gray - FACE-F/E0–E30); lines are model results.

Figure 13 summarizes the test results at the undiluted, lean condition where isopleths of τ = 4 ms are plotted for all of the fuel blends across the P-T space investigated at this fuel loading. While isopleths of τ covering 2–15 ms could be drawn from the dataset, only the τ = 4 ms lines are shown here, as this time has been found to reasonably correspond to onsets of HTHR during HCCI engine operation under scenarios where constant combustion phasing is employed, e.g., CA50 = 6 °aTDC (CA50 is the crank angle where 50% of the total measured heat release is recorded) [22, 36]. Both the simulated and measured RCM-based isopleths are constructed by interpolating the experimental or model results at each Tc where a power-law relation is assumed between τ and Pc, as shown by the insets of Fig. 12. Due to the discrepancies between the model and experiments, the simulated τ at the experimental conditions does not necessarily cover τ = 4 ms. Model results at these conditions are therefore not presented in Fig. 13. This is most evident for E30 since the model displays the largest disagreements for the E30 blends. It

should be noted again that the non-reactive Tc/Pc are used to obtain the results in Fig. 13 to mitigate against evolutions of exothermicity during piston compression. Measurement results for the full boiling range fuel blends are also included in Fig. 13 for reference [22].

In Fig. 13 it can be seen that at lower temperatures, higher pressures are required in order to maintain constant autoignition timings for E0, and this is similar to trends observed for engine operation [22]. The features of FGF-LLNL/E0 (Fig. 13a) in the experiments can be used to highlight this where starting from Tc = 1000 K a near-linear trend of Pc-Tc is followed, until an inflection point is reached at Tc = 940 K. This inflection point, which is fairly abrupt, is where the mixture enters the NTC regime [22] and two-stage heat release becomes observed at temperatures less than 870 K. The flux of reactants through low-temperature kinetic pathways at these conditions increases the overall fuel reactivity and leads to significantly altered temperature sensitivity. Comparing the 'neat' surrogates, it can be seen that the reactivity levels are fairly similar, except at the lowest compressed temperatures where FGF-LLNL/E0 is somewhat less reactive than FGF-KAUST/E0; this is slightly different than the behavior observed at the diluted/stoichiometric condition, indicating somewhat altered compositional effects. Overall, there appears to be fairly good correspondence between the 'neat' surrogate performance and the FACE-F/E0 results (gray symbols), where the FACE-F/E0 data are within the uncertainty estimates of the surrogate measurements.

The ethanol blending effects at the undiluted, lean condition are evident as shifts in the isopleths for the E10–E30 blends relative to the 'neat' fuels. As with the diluted/stoichiometric conditions, there is a significant temperature dependence of the ethanol response where, except at the highest temperatures, ethanol leads to progressively reduced reactivity as the

temperature is reduced. The low-temperature kinetic pathways and associated LTHR are suppressed such that substantially higher pressures are required to achieve the same combustion phasing. The responses in Pc required to maintain constant autoignition timing are summarized in Fig. S7 in the Supplementary Material where experimental and simulated relative pressures ($Pc^* = Pc/Pc_{neat}$) are plotted as functions of the compressed temperature, with the experimental results for the FACE-F/E0–E30 blends also included [22]. There it can be seen that both surrogates are affected by ethanol similarly in terms of the magnitudes of reactivity suppression at Tc < 970 K, as well as the level of reactivity enhancement at Tc > 970 K. The ethanol effects on the surrogates are also fairly consistent with the full boiling-range gasoline, except that the enhancement on FACE-F reactivity occurs at temperatures at Tc > 1000 K.

The model results shown in Fig. 13 reasonably captures the experimental measurements, but there are obviously quantitative discrepancies. For the 'neat' surrogates, it appears that the FGF-LLNL/E0 simulations are somewhat less reactive than the experiments, especially in the low-temperature/NTC regime, while the FGF-KAUST/E0 simulations fall within the experimental uncertainties for all experimental points except for the one at the highest temperature. The model also captures the qualitative differences between the neat surrogates. The ethanol blending responses predicted by the model, as quantified in Fig. S7, are somewhat muted however, where relative pressures are smaller than in the measurements, by ~6–12% (as shown in Fig. S8 in the Supplementary Material), with the difference increasing with the extents of ethanol in the fuel. The overpredicted reactivity by the model is consistent with the results at the diluted/stoichiometric condition. Additionally, as was observed in Fig. 7b, there do not appear to be significant differences between the ethanol-blended surrogates in the model.

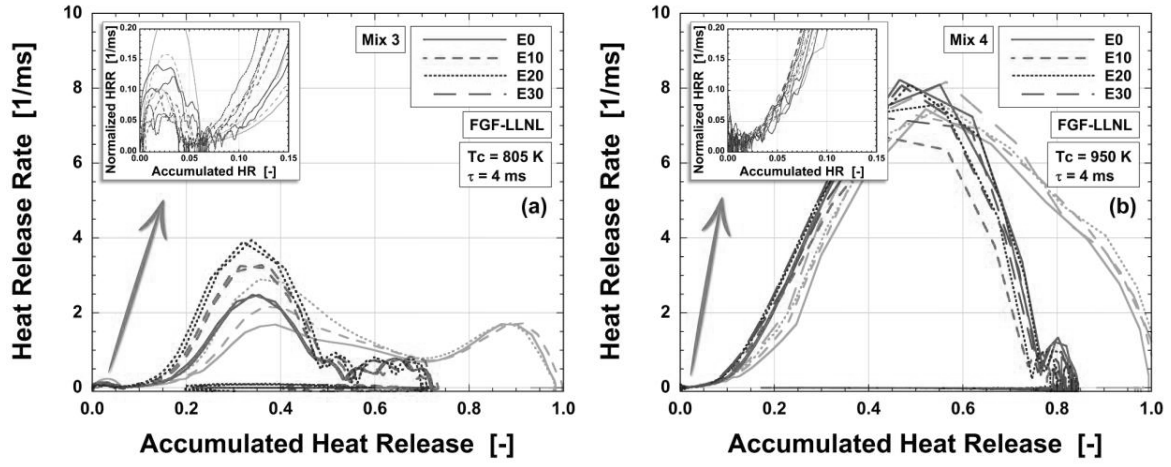

Figure 14. Calculated, normalized experimental and modeled heat release rates presented as functions of accumulated heat release for FGF-LLNL/E0-E30 blends at τ = 4 ms: (a) Tc = 805 K, Mix 3; (b) Tc = 950 K, Mix 4. Insets depict preliminary exothermicity with LTHR and ITHR demarcations identified, i.e., soITHR and soHTHR, respectively. Color lines are experimental results; gray lines are model results. Each mixture has two experimental curves that represent two reactive tests performed. The insets are provided as Supplementary Material (Fig. S9) to allow better interpretation of LTHR and ITHR between experiments and simulations.

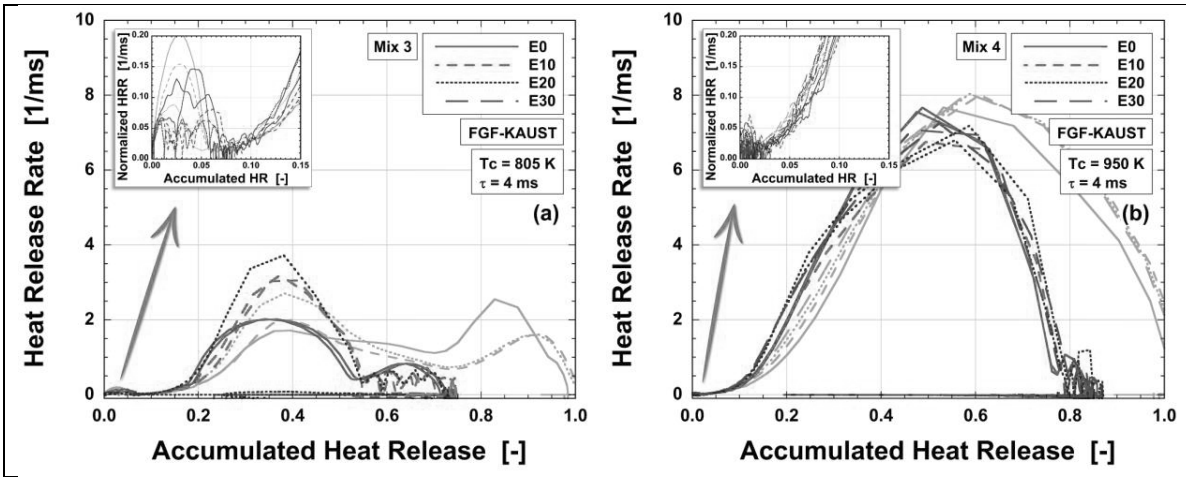

Figure 15. Calculated, normalized experimental and modeled heat release rates presented as functions of accumulated heat release for FGF-KAUST/E0-E30 blends at τ = 4 ms: (a) Tc = 805 K, Mix 3; (b) Tc = 950 K, Mix 4. Insets depict preliminary exothermicity with LTHR and ITHR demarcations identified, i.e., soITHR and soHTHR, respectively. Color lines are experimental results; gray lines are model results. Each mixture has two experimental curves that represent two reactive tests performed. The insets are provided as Supplementary Material (Fig. S10) to allow better interpretation of LTHR and ITHR between experiments and simulations.

Calculated, normalized experimental and modeled heat release rates are next presented in Figs. 14 and 15 as functions of accumulated heat release for FGF-LLNL/E0–E30 and FGF-KAUST/E0–E30, respectively, with $\tau \approx 4$ ms, and the same Tc conditions as in Fig. 12. It should be noted that at Tc = 805 K, the required Pc's range from 65 to 110 bar, with significantly greater Pc required at higher blending levels. Results for the E30 blends are not available at this temperature due to the excessive Pc required, which is beyond the hardware tolerances used in this study. At the Tc = 950 K, the Pc conditions for the E0–E30 blends are fairly similar due to their similar reactivity.

It is clear from Figs. 14 and 15 that FGF-LLNL/EtOH blends and FGF-KAUST/EtOH blends display similar HRR characteristics (e.g., LTHR behavior at Tc = 805 K, and multi-stage HTHR at both temperatures), with greater accumulated heat release seen at Tc = 950 K than at Tc = 805 K. Additionally, the peak HRRs at Tc = 950 K are greater than at the lower temperature due to the use of argon in the diluent. At Tc = 805 K (Fig. 14a and 15a), the differences between the 'neat' surrogates include somewhat faster transition to peak LTHR for FGF-LLNL/E0. LTHR is suppressed by ethanol blending, despite of the promoting effect on LTHR from significantly increased Pc's [22]. Additionally, there appears to be a reduction in total preliminary exothermicity with ethanol blending, which is different than that shown in Fig. 8a and 9a; this is most likely due to the different Pc's used along the isopleths. Furthermore, a shift in the first-stage of HTHR is evident with higher peak HRRs as ethanol is added, but it is unclear if this is due to ethanol-perturbed chemistry, or the higher Pc's used in the tests, since they have been found to both affect the multi-stage heat release characteristics [74]. Elucidating this requires quantification of the complex intermolecular interactions between ethanol and the surrogate

constituents, which is beyond the scope of this study, but will be included in a future study. Finally, at Tc = 950 K (Fig. 11b and 12b) where LTHR is non-existent, surrogate-to-surrogate differences and the influences of ethanol blending are negligible.

The model reasonably captures the surrogate-to-surrogate differences both with and without ethanol blending, such as the earlier evolution of LTHR and shifts in peak LTHR heat release rates. The trends are also analogous to those observed in Section 3.1. Consistent with the HRR characteristics observed in Fig. 9b and 10b, the model is able to replicate the qualitative trends in HRR, but over-predicts some of the accumulated heat release characteristics.

3.3. Sensitivity analysis

To draw further insight into surrogate-to-surrogate differences of ethanol blending effects, brute force sensitivity analysis is conducted on the main ignition delay time using constant volume simulations for E0 and E30 of FGF-LLNL and FGF-KAUST at and the same fuel loading conditions as in Section 3.1 and 3.2, and two compressed temperatures, namely Tc = 750 and 950 K, representative of low- and intermediate-temperature regimes, respectively. The sensitivity coefficients are defined as $S_{rel} = \ln\left(\frac{\tau^{\Delta}}{\tau}\right) / \ln\left(\frac{k^{\Delta}}{k}\right)$, where τ^{Δ} is the main ignition delay time after multiplying the original rate constant by 2, i.e.,. $k^{\Delta} = 2 * k$, and τ is the original ignition delay time. Negative sensitivity coefficients indicate that the reaction promotes reactivity, while positive coefficients indicate an inhibiting effect. Figure 16 and 17 present the computed sensitivity coefficients for the 20 most sensitive reactions for FGF-LLNL/EtOH and FGF-KAUST/EtOH blends, respectively, at the diluted/stoichiometric conditions, while the results at

the undiluted/lean condition are included in the Supplementary Material (Fig. S11 and S12). The species participating in these reactions can be identified in the species dictionary in the Supplementary Material.

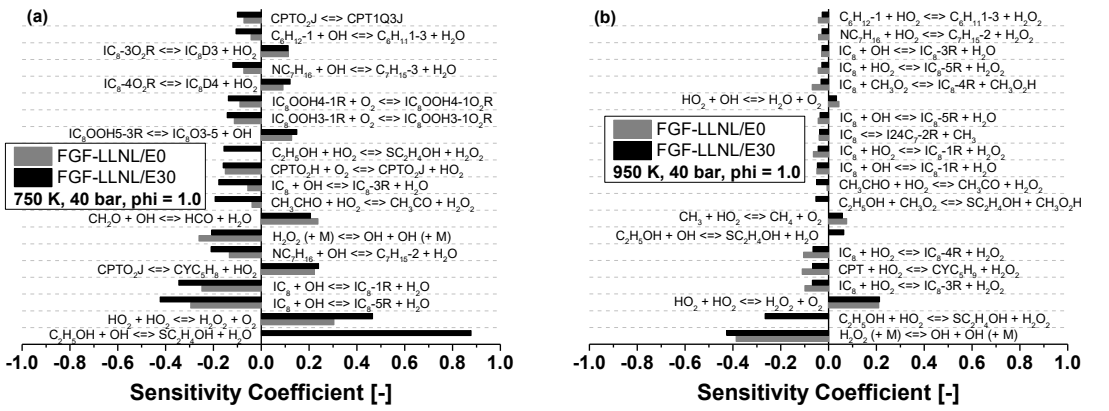

Figure 16. Sensitivity analysis on ignition delay time for FGF-LLNL/E0 and FGF-LLNL/E30 at Pc = 40 bar, and the diluted/stoichiometric condition; (a) Tc = 750 K and (b) 950 K. The participating species can be identified in the species dictionary in the supplementary material.

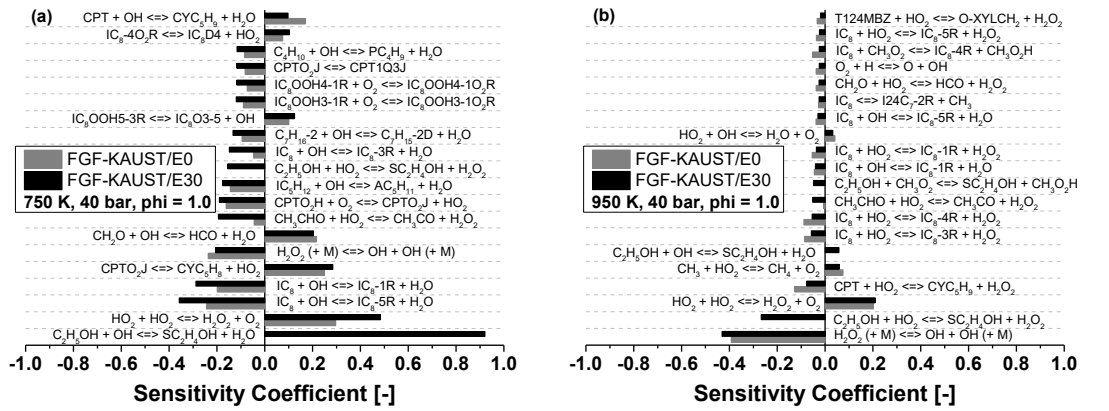

Figure 17. Sensitivity analysis on ignition delay time for FGF-KAUST/E0 and FGF-KAUST/E30 at Pc = 40 bar, and the diluted/stoichiometric condition; (a) Tc = 750 K and (b) 950 K. The participating species can be identified in the species dictionary in the supplementary material.

At Tc = 750 K (Fig. 16a and 17a), the most sensitive reactions for both FGF-LLNL/E0 and FGF-KAUST/E0 are typical low-temperature reaction classes, including H-atom abstraction from fuel molecule, concerted elimination of RO_2 radicals forming olefins and HO_2, intermolecular isomerization of RO_2 forming QOOH, cyclization of QOOH forming cyclic ether and ȮH, and O_2 addition to QOOH. Despite the compositional differences, the most sensitive reactions are dominated by iso-octane and cyclopentane chemistries for both surrogates, with contributions also from n-heptane and 1-hexane for FGF-LLNL/E0, and from 2-methyl butane, 2-methyl hexane, and n-butane for FGF-KAUST/E0. Particularly, the top four most sensitive reactions are consistent across the surrogates, with the most inhibiting reaction being $HO_2+HO_2<=>H_2O_2+O_2$. Ethanol blending effects are significant at this temperature, and consistent effects exhibit between the surrogates. First, with 30% vol. ethanol addition, the most inhibiting reaction becomes $C_2H_5OH+OH<=>SC_2H_4OH+H_2O$, which is the H-atom abstraction by ȮH on ethanol at α-site. This reaction significantly suppresses fuel reactivity because the produced SC_2H_4OH favors reaction channels yielding acetaldehyde and HO_2 radicals that are not reactive at low temperatures. Second, other reactions from ethanol chemistry also demonstrate significant sensitivities. For instance, doubling the rate constant of $C_2H_5OH+HO_2<=>SC_2H_4OH+H_2O_2$ enhances fuel reactivity greatly, resulting in a sensitivity coefficient of approximately -0.3. Additionally, there is a significant augment in the promoting effect of $CH_3CHO+HO_2<=>CH_3CO+H_2O_2$, as can be seen from Fig. 16a and 17a where the sensitivity coefficient of this reaction increases by at least five times when 30% ethanol is added. This is due to the increased yield of CH_3CHO from ethanol addition, primarily via $SC_2H_4OH+O_2<=>CH_3CHO+HO_2$.

With the updated ethanol chemistry (as discussed in Section 2.4), the sensitivity analysis results shown in Fig. 16a are different from those shown in [22] (Fig. 7a) in several aspects: 1) the magnitude of the coefficients is greater in this study, which is due likely to the updates implemented in ethanol sub-chemistry, and the changes in pressure condition and ethanol concentration; 2) the sensitivity of $CH_3CHO+HO_2=CH_3CO+H_2O_2$ is increased more significantly compared to [22] when more ethanol is blended (i.e., 30% vol. in Fig. 16a in this study vs. 20% vol. in Fig. 7a in [22]). This is an inhibiting, non-fuel-specific reaction where the participating species are contributed by several sub-chemistries, e.g., ethanol oxidation contributes significantly to CH_3CHO formation, while HO_2 and H_2O_2 can be massively produced from the surrogate chemistry. Adjusting the rate constant parameters of this type of reactions has the potential to reduce the model reactivity for ethanol-blended surrogates, while maintain similar reactivities for 'neat' surrogates, thus leading to improved agreements than those seen in Figs. 2 and 5. This requires further investigation, which is beyond the scope of this study.

At Tc = 950 K (Fig. 16b and 17b), results are also consistent between FGF-LLNL/E0 and FGF-KAUST/E0, where reactions involving HO_2 and H_2O_2 radicals become dominant. The most sensitive reactions are less fuel-dependent, with the top promoting and inhibiting reaction being $H_2O_2(+M)<=>OH+OH(+M)$ and $HO_2+HO_2<=>H_2O_2+O_2$, respectively, while the most sensitive fuel-specific reactions are the H-atom abstractions by HO_2 and, less importantly, ȮH radicals, which are again dominated by iso-octane chemistry. The abstraction reactions by HO_2 radical consistently promote reactivity as the produced H_2O_2 radical undergoes unimolecular decomposition to yield two ȮH radicals, leading the reaction pathway towards ȮH branching. Ethanol impacts are also significant at this temperature. For both E30 blends, the H-atom

abstraction by HO_2 forming α-hydroxyl ethanol radical, i.e., SC_2H_4OH, is the most promoting reaction among this reaction class. The results observed at diluted/stoichiometric condition are also consistent for the undiluted/lean condition.

3.4. Implications for current surrogate formulation strategies/methodologies.

In formulating the surrogates used in this work, the fuel reactivity was characterized targeting only the ASTM standardized properties of FACE-F such as RON, MON and S. Consequently, both surrogates represent FACE-F commendably in octane numbers (Table 2). Nevertheless, it remains unclear whether these surrogates are adequate to replicate FACE-F under conditions that are more representative of boosted/low-temperature combustion (LTC) and ACI engines, since fuel reactivity under such conditions has not been adequately captured by historical fuel metrics such as RON and MON. This open question is answered in the present study with the experimental observations directly comparing the 'neat' surrogates with FACE-F. Specifically, although both FGF-LLNL and FGF-KAUST display very similar behaviors to FACE-F, i.e., within the uncertainty estimates, at τ = 4 ms and the undiluted/lean fuel loading condition (Fig. 13), the obvious differences in their autoignition reactivity (Fig. 5) and LTHR characteristics (Fig. 9a and 10a) at the diluted/stoichiometric condition indicate that at least one of them does not replicate FACE-F properly at these conditions. Properly capturing the autoignition reactivity of the target gasoline across a wide range of engine-relevant conditions is necessary for high-fidelity surrogates due to the significant impact of autoignition reactivity on combustion characteristics. It is also important to capture the LTHR characteristics of the target gasoline since they have been

found to be critical to the ignition dynamics under various engine environments. For instance, in thermally-stratified/non-premixed combustion, LTHR is critical to the generation of low-temperature ignition kernels and cool flame/low-temperature ignition front, which subsequently affect the generation of high-temperature ignition kernels and propagating flames [75]. Also, LTHR at different stages of combustion process can lead to different combustion phenomena, e.g. LTHR at early stages of combustion process facilitate considerably advanced combustion phasing [76, 77], while those at later stages can cause localized events that may result in combustion noise or even knock [75]. However, such features have barely been considered in the application of current surrogate formulation strategies/methodologies. It is therefore recommended to include such fuel properties in addition to the standardized properties as targets for the formulation of high-fidelity gasoline surrogates.

On the other hand, current surrogate formulation strategies/methodologies for multi-component surrogates target only base gasolines without accounting for interactions with blending agents such as ethanol [22]. Surrogates designed with these constraints may not be adequate when blending behaviors are to be predicted. This is also demonstrated in this work by comparing the ethanol blending effects between FACE-F and its surrogates. Specifically, FGF-LLNL and FGF-KAUST were formulated targeting only FACE-F without considering the blending behavior with ethanol. As such, the surrogates do not fully replicate the ethanol blending effects on FACE-F, e.g., both surrogates display somewhat different responses to ethanol blending compared to FACE-F in both autoignition (Fig. 6a and 7a) and LTHR characteristics (Fig. 11a), particularly at conditions relevant to boosted/LTC engine operation. Surrogates formulated targeting only ‘neat’ gasolines have been extensively used in the past to generate fundamental

understanding and predict autoignition characteristics for gasoline blends with oxygenates. Given the discrepancies observed in this work, it is important to improve the current strategies/methodologies to achieve better accounting of blending effects. Including both the standardized and non-standardized properties as aforementioned of ethanol-blended gasolines complementary to those of 'neat' gasolines as target properties to be matched can be a potential way to achieve this.

The need for developing more accurate chemical models is also imperative. In [22], the increased disagreement between the model results and experiments at higher levels of ethanol blending was attributed to both the inadequacy in the surrogate makeup and the ethanol sub-chemistry including its interaction with the surrogate sub-chemistry. The former is confirmed in this work by Fig. 6a, 7a and 11a, where the surrogates' response to ethanol addition is somewhat different from FACE-F. However, the extents of difference in ethanol blending effects are considerably below the level of disagreement between the experiments and model results observed in Fig. 2 and 5, indicating that there are other significant contributors, i.e., the model inaccuracy. As discussed in Section 2.4, ethanol sub-chemistry in the chemical model has been further updated based on the findings in [22], aiming to achieve better agreement for the ethanol-blended surrogates. Although these updates led to excellent agreement for neat ethanol [48], the increased disagreement at higher levels of ethanol addition is still observed in this study for the surrogates (Fig. 2 and 5), and the level of disagreement is similar to those observed in [22] for FACE-F. This rules out the neat ethanol sub-chemistry, and indicates the improperly characterized interactions between the ethanol and surrogate sub-chemistries as the primary cause of the increasing disagreements. This is also confirmed when comparing several recent

studies, wherein the model showed relatively better agreement with the experiments for 'neat' FACE-LLNL [19], 'neat' FGF-KAUST [19] and neat ethanol [48], than for FGF-LLNL/EtOH and FGF-KAUST/EtOH blends as seen in this work. The insufficiency of the model in capturing the NTC behavior of the neat surrogates was also observed in [19], as well as in Fig. 5, which would most likely lead to consistent disagreement at different levels of ethanol blending, instead of the significantly elevated disagreement at higher levels of ethanol blending. Improvements of the chemical model are therefore needed in order to properly characterize the interactions between the ethanol and surrogate sub-chemistries.

Well-controlled conditions should be utilized for characterizing such interactions where physical influences such as fluid and gas dynamics are minimized, as are the thermal and compositional non-uniformities. Such conditions can be achieved in chemical reactors like RCM, shock tube and flow reactors. These facilities have been extensively used to probe the ethanol blending effects on neat hydrocarbons (e.g., n-heptane [26, 78], iso-octane [27, 79, 80] and toluene [81]), gasoline reference blends (e.g., primary reference fuels (PRFs) [81-83], toluene reference fuels (TRFs) [81] and multi-component surrogates used in this study), and full-boiling range gasolines [22], covering wide ranges of engine-relevant conditions. Almost all the studies to date have focused on changes to the ȮH and HO_2 radical pools that are altered via fuel-specific reactions (e.g., H-atom abstraction from ethanol) and hydrogen sub-chemistry (e.g., HO_2 recombination and H_2O_2 decomposition). Contributions due to intermolecular, non-fuel-specific reactions involving small-carbonated intermediates or radicals (e.g., formaldehyde, acetaldehyde and methyl radical) have not been discussed. Characterizing such interactions is however challenging since it requires quantifying the complex, non-fuel-specific intermolecular reactions

between ethanol and each surrogate constituent, and this is more difficult in multi-component surrogate blends. Furthermore, such reactions often involve a large number of small, important intermediates, including non-carbonated radicals such as OH, HO_2 and H_2O_2, and carbonated intermediates such as methyl radical and formaldehyde, which can alter the fuel reactivity considerably and be produced/consumed from different sub-chemistries. One example of such reaction can be seen in Section 3.3, where $CH_3CHO+HO_2=CH_3CO+H_2O_2$ is found to have significant impact on the main ignition reactivity of both surrogates at 30% vol. ethanol blending (Fig. 16a and 17a), and the production and consumption of these participating intermediates are contributed considerably from the sub-chemistries of both ethanol and the surrogate. Quantifying such non-fuel-specific intermolecular reactions is beyond the scope of this study, and will be included in a forthcoming study.

Multi-component gasoline surrogates can be formulated in CFR engines [28] targeting RON, MON and S. Such approach is less efficient and cost-effective since it requires vast experimental campaigns for each surrogate to be formulated. As such, multi-component surrogates, such as FGF-LLNL and FGF-KAUST, are typically formulated using chemical model as a foundation tool. These chemical models, however, have barely been validated directly against the surrogate experiments. Consequently, multi-component surrogates formulated targeting the same gasoline may display quite different behaviors. This is also seen in the present work, where FGF-LLNL and FGF-KAUST exhibit different ignition reactivity (Fig. 5) and heat release characteristics (Fig. 9a and 10a) although they are formulated targeting essentially the same set of standardized properties of FACE-F. This is due to the insufficiency of the model in capturing the surrogate-to-surrogate differences between the 'neat' surrogates (Fig. 2, 5–7, and 9–11), thus

highlighting the need of more extensive validations of the chemical models, particularly directly against the surrogates. Implementing such validations requires extensive physical testing on the surrogates, as well as their blends with ethanol in order to replicate also the blending behaviors, in well-controlled chemical reactors such as the RCM used in this study, where physical influences are minimized.

4. SUMMARY AND CONCLUSIONS

New experimental data are acquired for FGF-LLNL/E0-E30 and FGF-KAUST/E0-E30 in an RCM at diluted/stoichiometric and undiluted/lean fuel loadings, covering compressed temperature from 700 to 1000 K, and compressed pressure from 15 to 100 bar, respectively. A recently updated gasoline surrogate model is proposed and used to conduct relevant chemical kinetic modeling to help interpret the experimental measurements. Comprehensive analyses of the experimental and modeling results indicate the following:

- The diluted/stoichiometric experiments for both surrogates exhibit two-stage ignition/NTC behavior in the low-temperature regime, and single-stage ignition/Arrhenius behavior in the intermediate-temperature regime. Ethanol imposes only minor influences on ITHR and ignition reactivity for both surrogates within the intermediate temperature regime, but significantly suppresses LTHR and the low-temperature reactivity, with relatively greater perturbative effects demonstrated for FGF-LLNL than FGF-KAUST. The developed chemical model replicates the qualitative trends in autoignition and heat release characteristics,

with better agreement at intermediate temperatures, while relatively greater discrepancies are observed at higher levels of ethanol blending.

- Diluted/stoichiometric experiments also display surrogate-to-surrogate differences, where FGF-LLNL/E0 displays higher low-temperature reactivity and faster evolution of LTHR than FGF-KAUST/E0. Although this is not adequately captured by the model, flux analyses are able to reveal the compositional effects on first-stage ignition reactivity, where n-heptane initiates rapid OH branching at a faster rate and an earlier timing for FGF-LLNL/E0 than n-butane for FGF-KAUST/E0. Such differences are mostly muted by ethanol blending as ethanol scavenges the OH radicals from n-heptane oxidation that could otherwise initiate the oxidation of iso-octane and 1-hexene in FGF-LLNL.
- The undiluted/lean experiments, conducted under a constant combustion phasing scenario, display significant ethanol influences for both surrogates within the high-boost/low-temperature regime, where the surrogate-to-surrogate differences also display, with FGF-LLNL/E0 exhibiting somewhat less reactivity than FGF-KAUST/E0. Such trends are reasonably captured by the chemistry model.
- Despite the compositional difference, sensitivity analyses show similar dominating reactions between the surrogates, both with and without ethanol blending. When 30% vol. ethanol is blended to the surrogates, a significant augment in the importance for a non-fuel-specific, intermolecular reaction (e.g., $CH_3CHO+HO_2=CH_3CO+H_2O_2$) is observed, where the participating species can be produced/consumed from both the ethanol and surrogate sub-chemistries.

- Experimental observations directly comparing the surrogates and FACE-F suggest including non-standardized properties, such as first-stage and main ignition reactivity, and LTHR characteristics across a wide range of engine-relevant conditions rather than just RON- or MON-like/representative conditions, in addition to the conventional/standardized properties (e.g., RON, MON, C/H ratio, etc.), as targets to be matched for the formulation of high-fidelity surrogates that fully replicate the target gasoline.
- Differences in ethanol blending effects between the surrogates and FACE-F indicate the need to formulate high-fidelity surrogates that better account for ethanol-blending effects. This could be achieved by including the properties of gasoline/ethanol blends, complementary to those of 'neat' gasolines, as targets to be matched.
- The increasing disagreement between the experiments and model results at higher levels of ethanol blending is primarily caused by the inadequately characterized interactions between the ethanol and surrogate sub-chemistries, highlighting the need to quantify the complex, non-fuel-specific intermolecular reactions between ethanol and each surrogate constitute.
- The inadequacy of the chemical model in capturing the surrogate-to-surrogate differences suggests more extensive validation of the chemical model, directly against the surrogate experiments, which would require more physical testing of the surrogates in well-controlled chemical reactors.

5. ACKNOWLEDGEMENT

This manuscript has been created by UChicago Argonne, LLC, Operator of Argonne National Laboratory, a U.S. Department of Energy Office of Science laboratory, under Contract No. DE-AC02-06CH11357. The work at LLNL was performed under the auspices of the U.S. Department of Energy (DOE), Contract DE-AC52-07NA27344. The U.S. Government retains for itself, and others acting on its behalf, a paid-up nonexclusive, irrevocable worldwide license in said article to reproduce, prepare derivative works, distribute copies to the public, and perform publicly and display publicly, by or on behalf of the Government. The DOE will provide public access in accordance with http://energy.gov/downloads/doe-public-access-plan.

This research was conducted as part of the Partnership to Advance Combustion Engines (PACE) sponsored by the U.S. Department of Energy (DOE) Vehicle Technologies Office (VTO), and the Co-Optimization of Fuels and Engines (Co-Optima) initiative sponsored by the U.S. DOE Office of Energy Efficiency and Renewable Energy and Bioenergy Technologies, and VTO. Co-Optima is a collaborative project of multiple national laboratories initiated to simultaneously accelerate the introduction of affordable, scalable, and sustainable biofuels and high-efficiency, low-emission vehicle engines. Special thanks to program managers Kevin Stork, Gurpreet Singh, and Mike Weismiller.

The authors acknowledge the assistance of Dr. Jeffrey Santner, Dr. Toby Rockstroh and Mr. Tim Rutter for their efforts to maintain and operate ANL's tpRCM.

6. REFERENCE

[1] R.C.O.B. Delgado, A.S. Araujo, V.J. Fernandes, Properties of Brazilian gasoline mixed with hydrated ethanol for flex-fuel technology, Fuel Processing Technology 88 (2007) 365-368.

[2] M.D. Boot, M. Tian, E.J.M. Hensen, S. Mani Sarathy, Impact of fuel molecular structure on auto-ignition behavior – Design rules for future high performance gasolines, Progress in Energy and Combustion Science 60 (2017) 1-25.

[3] M.N. Nabi, H. Ogawa, N. Miyamoto, Nature of Fundamental Parameters Related to Engine Combustion for a Wide Range of Oxygenated Fuels, SAE International, 2002.

[4] M. Brusstar, M. Stuhldreher, D. Swain, W. Pidgeon, High Efficiency and Low Emissions from a Port-Injected Engine with Neat Alcohol Fuels, SAE International, 2002.

[5] U. Congress, Energy independence and security act of 2007, Public law 2 (2007) 110-140.

[6] J.T. Farrell, R. Wagner, D. Gaspar, C. Moen, Co-Optimization of Fuels & Engines: FY18 Year in Review, National Renewable Energy Lab.(NREL), Golden, CO (United States), 2019.

[7] J.E. Anderson, U. Kramer, S.A. Mueller, T.J. Wallington, Octane Numbers of Ethanol− and Methanol−Gasoline Blends Estimated from Molar Concentrations, Energy & Fuels 24 (2010) 6576-6585.

[8] T.M. Foong, K.J. Morganti, M.J. Brear, G. da Silva, Y. Yang, F.L. Dryer, The octane numbers of ethanol blended with gasoline and its surrogates, Fuel 115 (2014) 727-739.

[9] ASTM International, Standard Test Method for Research Octane Number of Spark-Ignition Engine Fuel, ASTM West Conshohocken, PA, D2699, 2007.

[10] ASTM International, Standard Test Method for Motor Octane Number of Spark-Ignition Engine Fuel, ASTM West Conshohocken, PA, D2700, 2013.

[11] J.C.G. Andrae, Development of a detailed kinetic model for gasoline surrogate fuels, Fuel 87 (2008) 2013-2022.

[12] J.C.G. Andrae, P. Björnbom, R.F. Cracknell, G.T. Kalghatgi, Autoignition of toluene reference fuels at high pressures modeled with detailed chemical kinetics, Combustion and Flame 149 (2007) 2-24.

[13] C. Pera, V. Knop, Methodology to define gasoline surrogates dedicated to auto-ignition in engines, Fuel 96 (2012) 59-69.

[14] M. Mehl, J.Y. Chen, W.J. Pitz, S.M. Sarathy, C.K. Westbrook, An Approach for Formulating Surrogates for Gasoline with Application toward a Reduced Surrogate Mechanism for CFD Engine Modeling, Energy & Fuels 25 (2011) 5215-5223.

[15] A. Ahmed, G. Goteng, V.S.B. Shankar, K. Al-Qurashi, W.L. Roberts, S.M. Sarathy, A computational methodology for formulating gasoline surrogate fuels with accurate physical and chemical kinetic properties, Fuel 143 (2015) 290-300.

[16] O.S. Abianeh, M.A. Oehlschlaeger, C.-J. Sung, A surrogate mixture and kinetic mechanism for emulating the evaporation and autoignition characteristics of gasoline fuel, Combustion and Flame 162 (2015) 3773-3784.

[17] W. Cannella, M. Foster, G. Gunter, W. Leppard, FACE gasolines and blends with ethanol: detailed characterization of physical and chemical properties, CRC Report No AVFL-24, (2014).

[18] S.M. Sarathy, G. Kukkadapu, M. Mehl, T. Javed, A. Ahmed, N. Naser, A. Tekawade, G. Kosiba, M. AlAbbad, E. Singh, S. Park, M.A. Rashidi, S.H. Chung, W.L. Roberts, M.A. Oehlschlaeger, C.-J. Sung, A. Farooq, Compositional effects on the ignition of FACE gasolines, Combustion and Flame 169 (2016) 171-193.

[19] D. Kang, A. Fridlyand, S.S. Goldsborough, S.W. Wagnon, M. Mehl, W.J. Pitz, M.J. McNenly, Auto-ignition study of FACE gasoline and its surrogates at advanced IC engine conditions, Proceedings of the Combustion Institute 37 (2019) 4699-4707.

[20] B. Chen, C. Togbé, H. Selim, P. Dagaut, S.M. Sarathy, Quantities of interest in jet stirred reactor oxidation of a high-octane gasoline, Energy & Fuels 31 (2017) 5543-5553.

[21] B. Chen, Z. Wang, J.-Y. Wang, H. Wang, C. Togbé, P.E.Á. Alonso, M. Almalki, M. Mehl, W.J. Pitz, S.W. Wagnon, K. Zhang, G. Kukkadapu, P. Dagaut, S. Mani Sarathy, Exploring gasoline oxidation chemistry in jet stirred reactors, Fuel 236 (2019) 1282-1292.

[22] S. Cheng, D. Kang, A. Fridlyand, S.S. Goldsborough, C. Saggese, S. Wagnon, M.J. McNenly, M. Mehl, W.J. Pitz, D. Vuilleumier, Autoignition behavior of gasoline/ethanol blends at engine-relevant conditions, Combustion and Flame 216 (2020) 369-384.

[23] J. Badra, A.S. AlRamadan, S.M. Sarathy, Optimization of the octane response of gasoline/ethanol blends, Applied Energy 203 (2017) 778-793.

[24] R. Vallinayagam, S. Vedharaj, N. Naser, W.L. Roberts, R.W. Dibble, S.M. Sarathy, Terpineol as a novel octane booster for extending the knock limit of gasoline, Fuel 187 (2017) 9-15.

[25] S.M. Sarathy, P. Oßwald, N. Hansen, K. Kohse-Höinghaus, Alcohol combustion chemistry, Progress in Energy and Combustion Science 44 (2014) 40-102.

[26] P. Dagaut, C. Togbé, Experimental and modeling study of the kinetics of oxidation of ethanol-n-heptane mixtures in a jet-stirred reactor, Fuel 89 (2010) 280-286.

[27] C.L. Barraza-Botet, M.S. Wooldridge, Combustion chemistry of iso-octane/ethanol blends: Effects on ignition and reaction pathways, Combustion and Flame 188 (2018) 324-336.

[28] H. Yuan, Y. Yang, M.J. Brear, T.M. Foong, J.E. Anderson, Optimal octane number correlations for mixtures of toluene reference fuels (TRFs) and ethanol, Fuel 188 (2017) 408-417.

[29] S.M. Sarathy, A. Farooq, G.T. Kalghatgi, Recent progress in gasoline surrogate fuels, Progress in Energy and Combustion Science 65 (2018) 67-108.

[30] M. Mehl, J.-Y. Chen, W.J. Pitz, S.M. Sarathy, C.K. Westbrook, An approach for formulating surrogates for gasoline with application toward a reduced surrogate mechanism for CFD engine modeling, Energy & Fuels 25 (2011) 5215-5223.

[31] S.M. Sarathy, G. Kukkadapu, M. Mehl, T. Javed, A. Ahmed, N. Naser, A. Tekawade, G. Kosiba, M. AlAbbad, E. Singh, Compositional effects on the ignition of FACE gasolines, Combustion and Flame 169 (2016) 171-193.

[32] A. Fridlyand, S.S. Goldsborough, M. Al Rashidi, S.M. Sarathy, M. Mehl, W.J. Pitz, Low temperature autoignition of 5-membered ring naphthenes: Effects of substitution, Combustion and Flame 200 (2019) 387-404.

[33] S.S. Goldsborough, J. Santner, D. Kang, A. Fridlyand, T. Rockstroh, M.C. Jespersen, Heat release analysis for rapid compression machines: Challenges and opportunities, Proceedings of the Combustion Institute 37 (2019) 603-611.

[34] J.B. Heywood, Internal combustion engine fundamentals, McGraw-Hill, New York, 1988.

[35] D. Vuilleumier, D. Kozarac, M. Mehl, S. Saxena, W.J. Pitz, R.W. Dibble, J.-Y. Chen, S.M. Sarathy, Intermediate temperature heat release in an HCCI engine fueled by ethanol/n-heptane mixtures: An experimental and modeling study, Combustion and flame 161 (2014) 680-695.

[36] T. Rockstroh, A. Fridlyand, S. Ciatti, W. Cannella, S.S. Goldsborough, Autoignition behavior of a full boiling-range gasoline: Observations in RCM and GCI engine environments, Combustion and Flame 209 (2019) 239-255.

[37] B.W. Weber, C.-J. Sung, M.W. Renfro, On the uncertainty of temperature estimation in a rapid compression machine, Combustion and Flame 162 (2015) 2518-2528.

[38] A. Fridlyand, M.S. Johnson, S.S. Goldsborough, R.H. West, M.J. McNenly, M. Mehl, W.J. Pitz, The role of correlations in uncertainty quantification of transportation relevant fuel models, Combustion and Flame 180 (2017) 239-249.

[39] S. Cheng, Y. Yang, M.J. Brear, M. Frenklach, Quantifying uncertainty in kinetic simulation of engine autoignition, Combustion and Flame 216 (2020) 174-184.

[40] M. Mehl, W.J. Pitz, C.K. Westbrook, H.J. Curran, Kinetic modeling of gasoline surrogate components and mixtures under engine conditions, Proceedings of the Combustion Institute 33 (2011) 193-200.

[41] Y. Li, C.-W. Zhou, K.P. Somers, K. Zhang, H.J. Curran, The oxidation of 2-butene: A high pressure ignition delay, kinetic modeling study and reactivity comparison with isobutene and 1-butene, Proceedings of the Combustion Institute 36 (2017) 403-411.

[42] M. Baigmohammadi, V. Patel, S. Nagaraja, A. Ramalingam, S. Martinez, S. Panigrahy, A.A.E.-S. Mohamed, K.P. Somers, U. Burke, K.A. Heufer, A. Pekalski, H.J. Curran, Comprehensive Experimental and Simulation Study of the Ignition Delay Time Characteristics of Binary Blended Methane, Ethane, and Ethylene over a Wide Range of Temperature, Pressure, Equivalence Ratio, and Dilution, Energy & Fuels 34 (2020) 8808-8823.

[43] Y. Zhang, H. El-Merhubi, B. Lefort, L. Le Moyne, H.J. Curran, A. Kéromnès, Probing the low-temperature chemistry of ethanol via the addition of dimethyl ether, Combustion and Flame 190 (2018) 74-86.

[44] G. Mittal, S.M. Burke, V.A. Davies, B. Parajuli, W.K. Metcalfe, H.J. Curran, Autoignition of ethanol in a rapid compression machine, Combustion and Flame 161 (2014) 1164-1171.

[45] A. Miyoshi, Systematic computational study on the unimolecular reactions of alkylperoxy (RO2), hydroperoxyalkyl (QOOH), and hydroperoxyalkylperoxy (O2QOOH) radicals, The Journal of Physical Chemistry A 115 (2011) 3301-3325.

[46] J. Lizardo-Huerta, B. Sirjean, R. Bounaceur, R. Fournet, Intramolecular effects on the kinetics of unimolecular reactions of β-HOROO$^{\cdot}$ and HOQ$^{\cdot}$ OOH radicals, Physical Chemistry Chemical Physics 18 (2016) 12231-12251.

[47] C. Saggese, C.M. Thomas, S.W. Wagnon, G. Kukkadapu, S. Cheng, D. Kang, S.S. Goldsborough, W.J. Pitz, An improved detailed chemical kinetic model for C3-C4 linear and iso-alcohols and their blends with gasoline at engine-relevant conditions, Proceedings of the Combustion Institute, doi:https://doi.org/10.1016/j.proci.2020.07.023.

[48] S. Cheng, D. Kang, S.S. Goldsborough, C. Saggese, S. Wagnon, W.J. Pitz, Experimental and modeling study of C2-C4 alcohol autoignition at intermediate temperature conditions, Proceedings of the Combustion Institute, doi:https://doi.org/10.1016/j.proci.2020.08.005.

[49] J. Bugler, B. Marks, O. Mathieu, R. Archuleta, A. Camou, C. Grégoire, K.A. Heufer, E.L. Petersen, H.J. Curran, An ignition delay time and chemical kinetic modeling study of the pentane isomers, Combustion and Flame 163 (2016) 138-156.

[50] K. Zhang, C. Banyon, J. Bugler, H.J. Curran, A. Rodriguez, O. Herbinet, F. Battin-Leclerc, C. B'Chir, K.A. Heufer, An updated experimental and kinetic modeling study of n-heptane oxidation, Combustion and Flame 172 (2016) 116-135.

[51] S.Y. Mohamed, L. Cai, F. Khaled, C. Banyon, Z. Wang, M.J. Al Rashidi, H. Pitsch, H.J. Curran, A. Farooq, S.M. Sarathy, Modeling ignition of a heptane isomer: improved thermodynamics, reaction pathways, kinetics, and rate rule optimizations for 2-methylhexane, The Journal of Physical Chemistry A 120 (2016) 2201-2217.

[52] R. Fang, G. Kukkadapu, M. Wang, S.W. Wagnon, K. Zhang, M. Mehl, C.K. Westbrook, W.J. Pitz, C.-J. Sung, Fuel molecular structure effect on autoignition of highly branched iso-alkanes at low-to-intermediate temperatures: Iso-octane versus iso-dodecane, Combustion and Flame 214 (2020) 152-166.

[53] S. Sharma, S. Raman, W.H. Green, Intramolecular Hydrogen Migration in Alkylperoxy and Hydroperoxyalkylperoxy Radicals: Accurate Treatment of Hindered Rotors, The Journal of Physical Chemistry A 114 (2010) 5689-5701.

[54] S.M. Villano, L.K. Huynh, H.-H. Carstensen, A.M. Dean, High-Pressure Rate Rules for Alkyl + O2 Reactions. 2. The Isomerization, Cyclic Ether Formation, and β-Scission Reactions of Hydroperoxy Alkyl Radicals, The Journal of Physical Chemistry A 116 (2012) 5068-5089.

[55] S.M. Villano, L.K. Huynh, H.-H. Carstensen, A.M. Dean, High-Pressure Rate Rules for Alkyl + O2 Reactions. 1. The Dissociation, Concerted Elimination, and Isomerization Channels of the Alkyl Peroxy Radical, The Journal of Physical Chemistry A 115 (2011) 13425-13442.

[56] A. Miyoshi, Molecular size dependent falloff rate constants for the recombination reactions of alkyl radicals with O2 and implications for simplified kinetics of alkylperoxy radicals, Int. J. Chem. Kinet. 44 (2012) 59-74.

[57] H.J. Curran, P. Gaffuri, W.J. Pitz, C.K. Westbrook, A comprehensive modeling study of iso-octane oxidation, Combustion and Flame 129 (2002) 253-280.

[58] H.J. Curran, P. Gaffuri, W.J. Pitz, C.K. Westbrook, A comprehensive modeling study of n-heptane oxidation, Combustion and Flame 114 (1998) 149-177.

[59] M. Mehl, W.J. Pitz, C.K. Westbrook, K. Yasunaga, C. Conroy, H.J. Curran, Autoignition behavior of unsaturated hydrocarbons in the low and high temperature regions, Proceedings of the Combustion Institute 33 (2011) 201-208.

[60] G.M. Chupka, E. Christensen, L. Fouts, T.L. Alleman, M.A. Ratcliff, R.L. McCormick, Heat of vaporization measurements for ethanol blends up to 50 volume percent in several hydrocarbon blendstocks and implications for knock in SI engines, SAE International Journal of Fuels and Lubricants 8 (2015) 251-263.

[61] N. Lokachari, S.W. Wagnon, G. Kukkadapu, W.J. Pitz, H.J. Curran., An experimental and kinetic modelling study of cyclopentane and dimethyl ether blends, Combustion and Flame 161 (2014) 2739-2751.

[62] G. Kukkadapu, D. Kang, S.W. Wagnon, K. Zhang, M. Mehl, M. Monge-Palacios, H. Wang, S.S. Goldsborough, C.K. Westbrook, W.J. Pitz, Kinetic modeling study of surrogate components for gasoline,

jet and diesel fuels: C7-C11 methylated aromatics, Proceedings of the Combustion Institute 37 (2019) 521-529.

[63] B. Ruscic, D. Bross, Active Thermochemical Tables (ATcT) values based on ver. 1.122 of the Thermochemical Network, ATcT. anl. gov, (2016).

[64] C.F. Goldsmith, G.R. Magoon, W.H. Green, Database of Small Molecule Thermochemistry for Combustion, The Journal of Physical Chemistry A 116 (2012) 9033-9057.

[65] E.R. Ritter, J.W. Bozzelli, THERM: Thermodynamic property estimation for gas phase radicals and molecules, 23 (1991) 767-778.

[66] W.H. Green, R.H. West, RMG – Reaction Mechanism Generator (2020) http://rmg.mit.edu/.

[67] D. Chen, K. Wang, H. Wang, Violation of collision limit in recently published reaction models, Combustion and Flame 186 (2017) 208-210.

[68] N.J. Killingsworth, M.J. McNenly, R.A. Whitesides, S.W. Wagnon, Cloud based tool for analysis of chemical kinetic mechanisms, Combustion and Flame 221 (2020) 170-179.

[69] B.J. McBride, S. Gordon, M.A. Reno, Coefficients for Calculating Thermodynamic and Transport Properties of Individual Species; National Aeronautics and Space Administration (NASA): Washington, D.C., 1993; NASA Technical Memorandum 4513.

[70] S. Dooley, M. Uddi, S.H. Won, F.L. Dryer, Y. Ju, Methyl butanoate inhibition of n-heptane diffusion flames through an evaluation of transport and chemical kinetics, Combustion and Flame 159 (2012) 1371-1384.

[71] R. Bosque, J. Sales, Polarizabilities of Solvents from the Chemical Composition, Journal of Chemical Information and Computer Sciences 42 (2002) 1154-1163.

[72] M.J. McNenly, R.A. Whitesides, D.L. Flowers, Faster solvers for large kinetic mechanisms using adaptive preconditioners, Proceedings of the Combustion Institute 35 (2015) 581-587.

[73] S.S. Goldsborough, S. Hochgreb, G. Vanhove, M.S. Wooldridge, H.J. Curran, C.-J. Sung, Advances in rapid compression machine studies of low- and intermediate-temperature autoignition phenomena, Progress in Energy and Combustion Science 63 (2017) 1-78.

[74] A.S. AlRamadan, R.M. Galassi, P.P. Ciottoli, M. Valorani, S.M. Sarathy, Multi-stage heat release in lean combustion: Insights from coupled tangential stretching rate (TSR) and computational singular perturbation (CSP) analysis, Combustion and Flame 219 (2020) 242-257.

[75] A. Krisman, E.R. Hawkes, J.H. Chen, A parametric study of ignition dynamics at ECN Spray A thermochemical conditions using 2D DNS, Proceedings of the Combustion Institute 37 (2019) 4787-4795.

[76] D.A. Splitter, A. Gilliam, J. Szybist, J. Ghandhi, Effects of pre-spark heat release on engine knock limit, Proceedings of the Combustion Institute 37 (2019) 4893-4900.

[77] G.S. Jatana, D.A. Splitter, B. Kaul, J.P. Szybist, Fuel property effects on low-speed pre-ignition, Fuel 230 (2018) 474-482.

[78] P. Saisirirat, C. Togbé, S. Chanchaona, F. Foucher, C. Mounaim-Rousselle, P. Dagaut, Auto-ignition and combustion characteristics in HCCI and JSR using 1-butanol/n-heptane and ethanol/n-heptane blends, Proceedings of the Combustion Institute 33 (2011) 3007-3014.

[79] H. Song, H. Song, Ignition delay measurements of iso-octane/ethanol blend fuel in a rapid compression machine, Proceedings of the European combustion meeting, (2015).

[80] Z. Lu, Y. Yang, M.J. Brear, Impact of ethanol on oxidation of iso-octane at low and intermediate temperatures, Combustion and Flame 214 (2020) 167-183.

[81] H. Yuan, Z. Lu, Z. Chen, Y. Yang, M.J. Brear, J.E. Anderson, T. Leone, Oxidation of ethanol and hydrocarbon mixtures in a pressurised flow reactor, Combustion and Flame 199 (2019) 96-113.

[82] Q. Fan, Z. Wang, Y. Qi, Y. Wang, Investigating auto-ignition behavior of n-heptane/iso-octane/ethanol mixtures for gasoline surrogates through rapid compression machine measurement and chemical kinetics analysis, Fuel 241 (2019) 1095-1108.

[83] E. Singh, E.-A. Tingas, D. Goussis, H.G. Im, S.M. Sarathy, Chemical ignition characteristics of ethanol blending with primary reference fuels, Energy & Fuels 33 (2019) 10185-10196.